NTNU

Norwegian University of
Science and Technology

Calculation of NOx Formation in a Swirl Burner

Andreas Fiskum

Master of Science in Product Design and Manufacturing
Submission date: June 2008
Supervisor: Johan Einar Hustad, EPT

Norwegian University of Science and Technology
Department of Energy and Process Engineering

Problem Description

Flow patterns, mixing, temperature and emissions in a swirl burner with varying geometry and partially premixing are to be calculated. Discussion about how the above-mentioned parameters affect the calculation results are to be included. The work shall serve as background experience for subsequent experimental verification and shall therefore result in recommendations for testing of partial premixing in a swirl burner.

Assignment given: 18. January 2008
Supervisor: Johan Einar Hustad, EPT

Preface

The work described in this report is the result of my master thesis performed at the Norwegian University of Science and Technology in Trondheim. The report is written for the Department of Energy and Process Engineering.

I would like to thank my academic supervisor Professor Johan Einar Hustad for his guidance and support. I would also want to thank my co-supervisor Dr. Ing. Øystein Spangelo, who used his spare time to help me with both theoretical and data based problems. Gratitude should also be given to the technical personnel here at NTNU, who assisted me when the computer and FLUENT refused to cooperate.

At last I would like to thank my fellow students for the academic breaks through this semester. My card-playing skills will never be better than they are now.

Trondheim, June 2008

Andreas Fiskum

Abstract

This thesis embraces simulations of NO_x emissions from a partially premixed 20 kW swirl burner. The simulations were carried out in the commercial computational fluid dynamics software FLUENT. The concept of partial premixing air and fuel before adding additional air for complete combustion has proven promising with a view on the NO_x emissions. However, little research has been done on rich premixing of fuel and air and therefore further investigation of this topic is of interest. In most experiments in the literature methane is used as fuel, but due to problems with stability and blow off in the 20 kW swirl burner propane were chosen as fuel.

Simulations of eight different air-fuel ratios have been performed, ranging from diffusion flame to a mass based air-fuel ratio of four. The results from the simulation with no premixing proved satisfactory when comparing with previous experimental and simulated work, except from the calculation of the exact NO_x concentration. This difference in the concentration was one the other hand expected since the power of FLUENT and similar software is to predict variation trends and not the exact value itself.

The simulations showed that the NO_x concentration increased with increasing premixing, reaching a local peak at an air-fuel ratio of two. After this a local minimum in the NO_x concentration was observed before a strong increase when further raising the air-fuel ratio. This is the same trends that are observed in the literature when using methane as fuel, but for propane there is no global reduction in the NO_x emissions when applying premixing. This increase in the NO_x emission was found to be due to an expansion of the high temperature flame zone with increasing premixing, which benefits the thermal NO_x formation mechanism. The NO_x reducing effect of swirl generation was observed to decrease when the air-fuel ratio was increased.

For subsequent experimental work it is recommended to perform a high amount of experiments at different air-fuel ratios, especially in the ratio range where the NO_x concentrations starts to fluctuate. Effort should also be made to find the temperature distribution in the combustion chamber at different air-fuel ratios. This will help verify the simulations where partial premixing was implemented.

Sammendrag

Denne rapporten tar for seg simuleringer av NO_x-utslippet fra en partiell premikset 20 kW swirlbrenner. Simuleringen ble utført ved bruk av det kommersielle analyseprogrammet FLUENT. Prinsippet med å partielt premikse luft og brensel før ytterlig luft er tilført for forbrenning har vist seg som en lovende NO_x reduserende teknikk. Lite undersøkelser har blitt gjort rundt temaet rik forblanding av luft og brensel, og nærmere undersøkelser på effekten av denne typen forblanding er derfor interessant. I litteraturen er de fleste eksperimenter utført med metan som brensel, men på grunn av driftproblemer på den brenneren som er beskrevet i denne rapporten ble propan foretrukket som brensel.

Simuleringer av åtte forskjellige luft/brensel-forhold har blitt gjennomført, fra diffusjonsflamme til et forblandingsforhold på fire. Resultatene fra simuleringen uten premiksing viste seg tilfredsstillende når de ble sammenlignet med tidligere eksperimenter og simuleringer som er gjort på den samme swirlbrenneren, bortsett fra beregningen av den eksakte NO_x-konsentrasjonen. Den forskjellen var derimot forventet, siden styrken til FLUENT og lignende programvare er å beregne variasjoner og ikke eksakte verdier.

Simuleringen viste at NO_x konsentrasjonen økte ved økt grad av premiksing, og en lokal topp ble observert ved et luft/brensel-forhold på to. Ved videre økning av forblandingsforholdet var det først en liten nedgang i konsentrasjonen før det igjen økte kraftig. Dette er det samme mønsteret som tidligere er observert ved bruk av metan som brensel, men forskjellen er at propan ikke har noen global reduksjon av NO_x-utslippet når premiksing implementeres. Årsaken til denne økningen i NO_x-utslipp var blant annet et økt høytemperaturområde i brennkammeret ved økt premiksing, noe som favoriserer termisk NO_x-produksjon. Effekten av NO_x-reduseringen som swirlgeneratoren står for ble i tillegg redusert ved økende forblandingsforhold.

For videre eksperimentelt arbeid på samme felt er det anbefalt å utføre et stort antall forsøk ved forskjellige luft/brensel-forhold, spesielt i området hvor NO_x-konsentrasjonen starter å fluktuere. The bør også gjennomføres målinger av temperaturfordelingen i brennkammeret ved forksjellige luft/brensel-forhold. Resultatene fra temperaturmålingene kan være med på å verifisere de simuleringene hvor premiksing er implementert.

Table of contents

List of figures

List of tables

Nomenclature

Arabic:

A	Area	[m^2]
A	Constant	
B	Constant	
C	Constant	
d	Diameter	[m]
D	Diffusion coefficient	
DFR	Diluent-to-fuel ratio	
E_a	Activation energy	[J/mol]
f	Correction factor	
f	External body force	[kg/m^2-s]
FAR	Fuel-air ratio	
G	Stochastic variable	
G	Flux	[kg-m/s]
h	Enthalpy	[J/kg]
j	Diffusion flux	
k	Turbulent kinetic energy	[m^2/s^2]
k	Rate coefficient	[m^3/kmol-s]
L	Length scale	[m]
LFL	Lower flammability limit	[vol%]
LHV	Lower heating value	[MJ/kg]
m	mass	
MW	Molecular weight	[kg/kmol]
n	Amount of mol	[mol]
n	Sample number n	
N	Total amount of samples	
p	Pressure	[bar]
P	Pressure	[bar]
P	Turbulent kinetic energy	
P	Power	[kW]
ppmv	Parts per million by volume	
Q_{EAS}	Skewness of mesh elements	
r	Radius	[m]
R	Production rate	
R	Universal gas constant	[J/mol-K]
S	Swirl number	
S	Source term	
t	time	[s]
T	Temperature	[˚C]
T	Temperature	[K]
tan	Tangent	
u	Velocity	[m/s]

UFL	Upper flammability limit	[vol%]
v	Velocity	[m/s]
v	Stoichiometric oxidiser to fuel mass ratio	
x	x-coordinate	
Y	Mass fraction	

Greek:

α	Thermal viscosity	[$^{\circ}C^{-1}$]
β	Exit angle, swirl vanes	[$^{\circ}$]
δ	Identity matrix	
ε	Dissipation of turbulent energy	[m^2/s^3]
θ	Angle between the edge of a mesh element	[$^{\circ}$]
λ	Excess air ratio	
φ	Stochastic fluid property	
ϕ	Overall combustion equivalence ratio	
ϕ_{local}	Gas tube equivalence ratio	
Φ	Pressure-strain term	
ρ	Density	[kg/m^3]
σ	Constant	
τ	Stress tensor	[$kg/m\text{-}s^2$]
μ	Viscosity	[kg/m-s]
ξ	Characteristic variable	
π	Non-conserved property	

1 Introduction

This master thesis focuses on nitrogen oxides (NO_x) reduction techniques. NO_x is an unwanted product of a combustion process and can cause health and environmental impacts like ground-level ozone, acid rain, particles, water quality deterioration, climate change, toxic chemicals and visibility impairment [1]. In accordance with the Gothenburg protocol, Norway is obliged to reduce the emissions of NO_x to 156 000 tonnes in 2010. To reach this level, a reduction of 35 000 tons (18%) from the 2006 emissions has to be made. To put the necessary reduction into perspective; from 1990 to 2006 Norway reduced the emissions of NO_x with 8 %. Therefore, a great effort has to be made if the emission level from the Gothenburg protocol is to be reached. The largest source of NO_x emissions was in 2006 the domestic sea transport and fishing, accounting for 34% of the total. The second largest source is the oil and gas sector, which contributed with 27% of the total. The emissions from oil and gas activities have increased with 72% since 1990, and are one of the reasons that Norway struggles to reach the emission limit in accordance with the Gothenburg protocol [2].

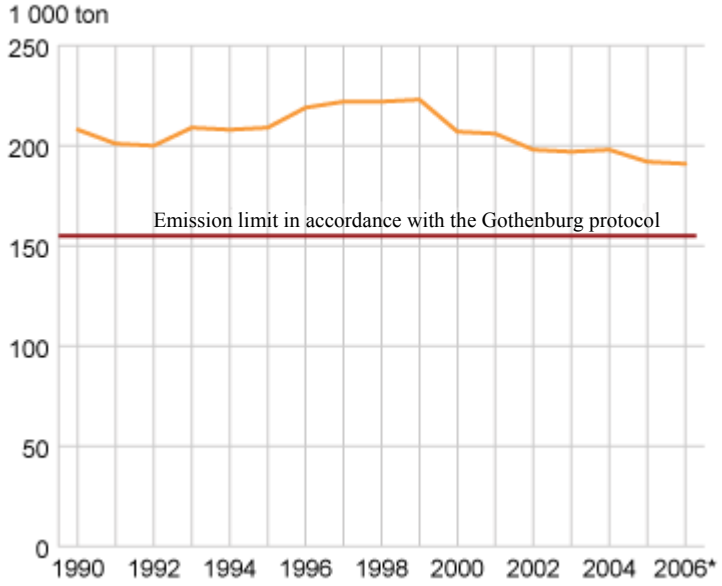

Figure 1: NO_x emissions in Norway from 1990 to 2006 [2]

One possible measure to reduce the emissions in the oil and gas sector is to introduce low-NO_x turbines in the power generators. There exist several low-NO_x techniques but due to the cost of retrofitting old process installations, most of these techniques are not economical feasible. Therefore, finding a NO_x reducing technique that can be implemented into an existing installation without comprehensive retrofitting is of great interest.

One promising low-cost NO_x reducing technique is to partially premix air and fuel before adding additional air for complete combustion. A schematic view of the concept is given

in Figure 2. This concept can be implemented into an existing burner with a relatively little need of reconstruction.

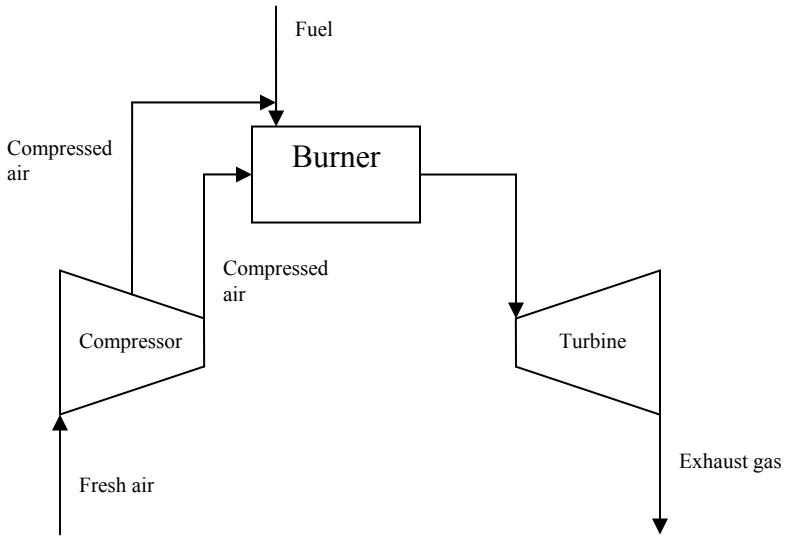

Figure 2: Schematic view of the partially premixed air-fuel concept

The aim of this master thesis is to examine what effect partial premixing have on the NO_x emissions with the use of commercial computational fluid dynamics (CFD) software. The burner modeled is a 20 kW swirl burner designed by Øystein Spangelo [3], and the simulations were performed in the CFD software FLUENT. The results of the simulations are compared with theory from the literature, experiments and previous simulations done on the same burner.

2 Literature and theory

When working with the topic NO_x reduction experiments with the use of CFD software, it is important to understand both the NO_x formation mechanisms and the limits of CFD. Therefore this chapter will give an introduction to the different NO_x formation mechanisms and the equations and models used in the CFD software. An overview over different NO_x reducing techniques will also be given.

2.1 NO_x formation mechanisms

The term NO_x stands for the two most common nitrogen oxides produced during combustion, NO and NO_2. These two species are often treated together based on the assumption that the dominating component, NO, oxidizes to NO_2 either in the atmosphere or in the industrial device. In combustion of fuels that contain little or no nitrogen, nitrogen oxides is formed by four mechanisms that involve nitrogen from the air: the thermal mechanism, the prompt mechanism, the N_2O-intermidediate mechanism and the NNH mechanism. To be able to control emissions of nitrogen oxides, it is important to understand the different chemical mechanisms producing NO_x in combination with fluid dynamics. The different mechanisms will be discussed in the following sections.

The **thermal mechanism,** also referred to as the extended Zeldovich mechanism, can be simplified to the following elementary reactions:

$$O + N_2 \Leftrightarrow NO + N \tag{2-1}$$

$$N + O_2 \Leftrightarrow NO + O \tag{2-2}$$

$$N + OH \Leftrightarrow NO + H \tag{2-3}$$

The rate-limiting reaction is equation (2-1) due to its relatively high activation energy of 319 050 kJ/kmol [4]. With the assumptions that the N_2, O_2, O and OH concentrations are at their equilibrium values, the NO concentrations are much less than their equilibrium values and the N atoms are in steady state, the following expression can be obtained [4]:

$$\frac{d[NO]}{dt} = 2k_1[O]_{eq}[N_2]_{eq} \tag{2-4}$$

Where [] denote concentrations and k_1, the rate coefficient in equation (2-1), is given by:

$$k_1 = 1,8 \cdot 10^{11} \cdot \exp\left[\frac{-38370}{T(K)}\right] = \left[\frac{m^3}{kmol - s}\right] \tag{2-5}$$

From equation (2-4) and (2-5), it can be seen that the thermal NO formation can be controlled by the O and N_2 concentration, temperature and residence time. Thus by preventing hot spots, reducing oxygen rich zones at high temperatures and reducing time

of exposure at high temperatures can lower the NO_x production. In the literature, thermal NO_x is said to be unimportant for temperatures below 1800 K [4, 5].

The **prompt mechanism**, also known as the Fenimore mechanism, is directly linked to the combustion of hydrocarbons. Hydrocarbon radicals react with molecular nitrogen to form hydrocyanic acid (HCN). These compounds are then converted to intermediate compounds that form NO. The quantity of HCN formed increases with the concentration of hydrocarbon radicals, which in turn increases with equivalence ratio. The prompt mechanism can be described with the following equations [3]:

$$N_2 + CH \Leftrightarrow HCN + N \quad (2\text{-}6)$$

$$HCN + O \Leftrightarrow NCO + H \quad (2\text{-}7)$$

(2-6) and (2-7) will ultimately react to form NO, and the chemistry becomes more complex with higher equivalence ratio. As the equivalence ratio increases, prompt NOx production increases at first, then passes a peak, and finally decreases due to a deficiency in oxygen [6].

The **N_2O-intermediate mechanism** increases in importance under fuel-lean, low temperature and high pressure conditions. The following three reactions are involved in the N_2O-intermediate mechanism [4]:

$$O + N_2 + M \Leftrightarrow N_2O + M \quad (2\text{-}8)$$

$$H + N_2O \Leftrightarrow NO + NH \quad (2\text{-}9)$$

$$O + N_2O \Leftrightarrow NO + NO \quad (2\text{-}10)$$

This mechanism becomes important in lean premixed combustion, but may also contribute to the NO_x-production in rich premixed combustion [4].

The **NNH mechanism** is a route forming NO by the oxidation of NNH radicals proposed by Bozzelli and Dean in 1995 [7]. They suggested that significant amounts of nitrogen oxide can be produced in flames from N_2 via NNH formed in the reactions:

$$N_2 + H \Leftrightarrow NNH \quad (2\text{-}11)$$

$$NNH + O \Leftrightarrow NH + NO \quad (2\text{-}12)$$

This route is said to be of importance in rich flames and in lean mixtures up to moderately high (1900 K) temperatures [8].

Another nitrogen oxide mechanism is the conversion of fuel bound nitrogen to NO. This mechanism is not considered to be of importance in the problem described in this thesis because of the use of clean fuels like methane and propane that contain no nitrogen.

2.2 NO_x reducing techniques

When reducing NO_x emissions from combustion processes, the methods used are often separated into two main procedures, named primary and secondary measures. The secondary measures focus on treatment of the flue gas, instead of reducing the formation of the pollutants. Examples of secondary measures are catalytic reduction and reactions with for instance ammonia. Secondary measures are economical expensive and technically challenging and therefore a lot of effort has been made to reduce the NO_x where it is produced, called primary measures. This thesis focuses on primary measuring techniques, and for that reason some well known methods to reduce NO_x in burners will be explained in the following sections.

2.2.1 Staged combustion

The NO_x emission is at its peak at stoichiometric conditions when other pollutants, like CO and VOC, is at its minimum (see Figure 3). This is mainly because of the strong relation between temperature and thermal NO_x production as explained in chapter 2.1.

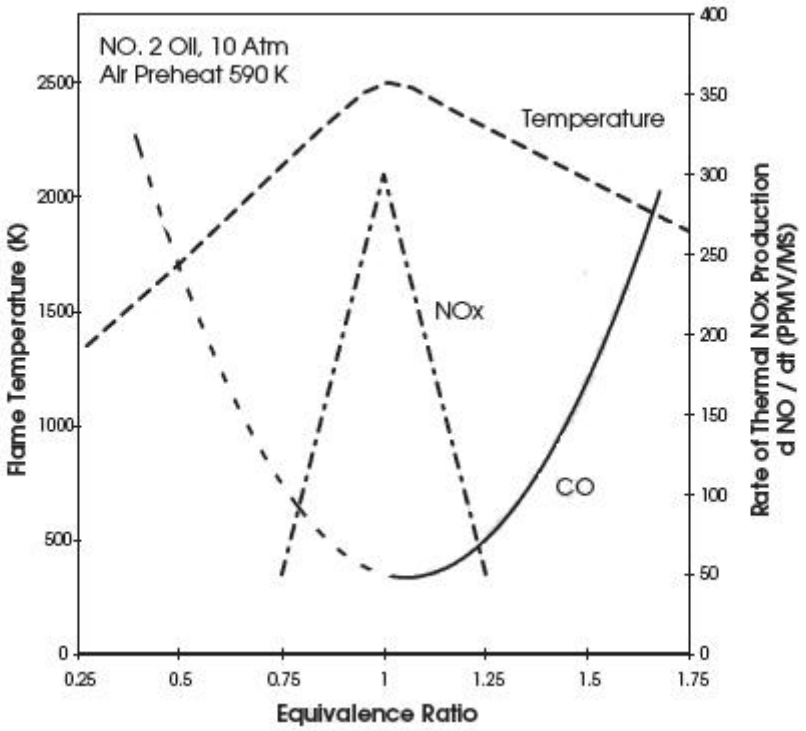

Figure 3: NO_x formation rate driven by temperature [9]

There are two ways to accomplish staged combustion, referred to as air and fuel staging (see Figure 4). The idea of air staged combustion is first to take advantage of the stability and low NO_x production associated with rich combustion ($\lambda < 1$), and subsequently break down the unburned CO an H_2 in a lean combustion ($\lambda > 1$). Fuel staging is in principal the same, but then the combustion is first very lean and subsequently more fuel is added to make the mix less lean.

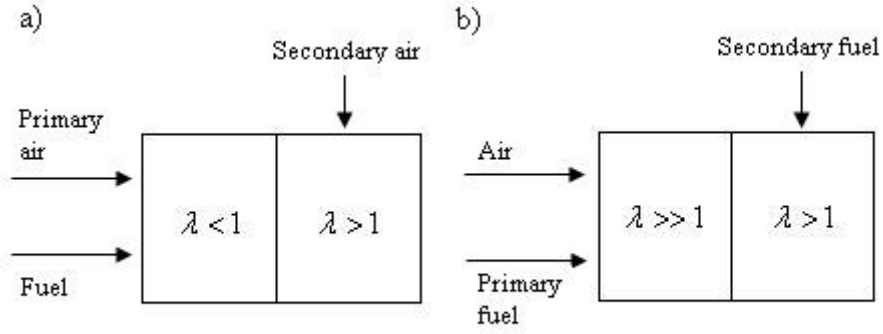

Figure 4: Schematic drawing of (a) air staging, and (b) fuel staging [3]

2.2.2 Partially premixed flames

Partially premixed flames are established when less than stoichiometric quantity of oxidizer is molecularly mixed with the fuel stream before entering the reaction zone where additional oxidizer is available for complete combustion. The aim of this is to ensure that the fuel and air is perfectly molecular mixed before the ignition takes place. Good mixing of the fuel and air enables better control over the air and fuel ratio throughout the combustion, which again gives an improved control of the combustion temperature [3]. When the amount of partial premixing increases (more air premixed with the fuel) the combustion temperature increases, leading to shorter residence time and a possible reduction in the NO_x emissions [10].

Experimental studies have shown that there exists an optimum level of partial premixing that will give the lowest NO_x emissions, for a fixed fuel flow rate and overall equivalence ratio with methane as fuel [11-14]. For Methane-air combustion, a minimum NO_x emission with an equivalence ratio (ϕ_{local} [1]) in the fuel rich zone of $1.5 < \phi_{local} < 3$ is observed [11, 12, 14]. The relatively large differences in ϕ for the studies referred to here may come of different strain rates in the experiments [13]. In the study carried out by Gore and Zhan the $EINO_x$ is approximately constant when going from a diffusion flame to $\phi_{local} \approx 4$, then subsequently drop to a minimum at $\phi_{local} \approx 2$ and then increase as ϕ_{local} reaches the upper flammability limit (see Figure 5). This is also observed in the experiments performed by Cheng et al. [11]. Another characteristic that is observable in Cheng's experiments is when going from diffusion flame to partially premixed flame there is a peak in the NO_x emissions in the area $\phi_{local} \in [4, \infty]$. This implies that not all premix ratios gives reduction in NO_x emissions.

[1] The equivalence ratio with subscript "local" is referred to as the ratio before reaction with oxygen, i.e. in the premixed fuel-air pipe. The equivalence ratio is described in chapter 2.3.

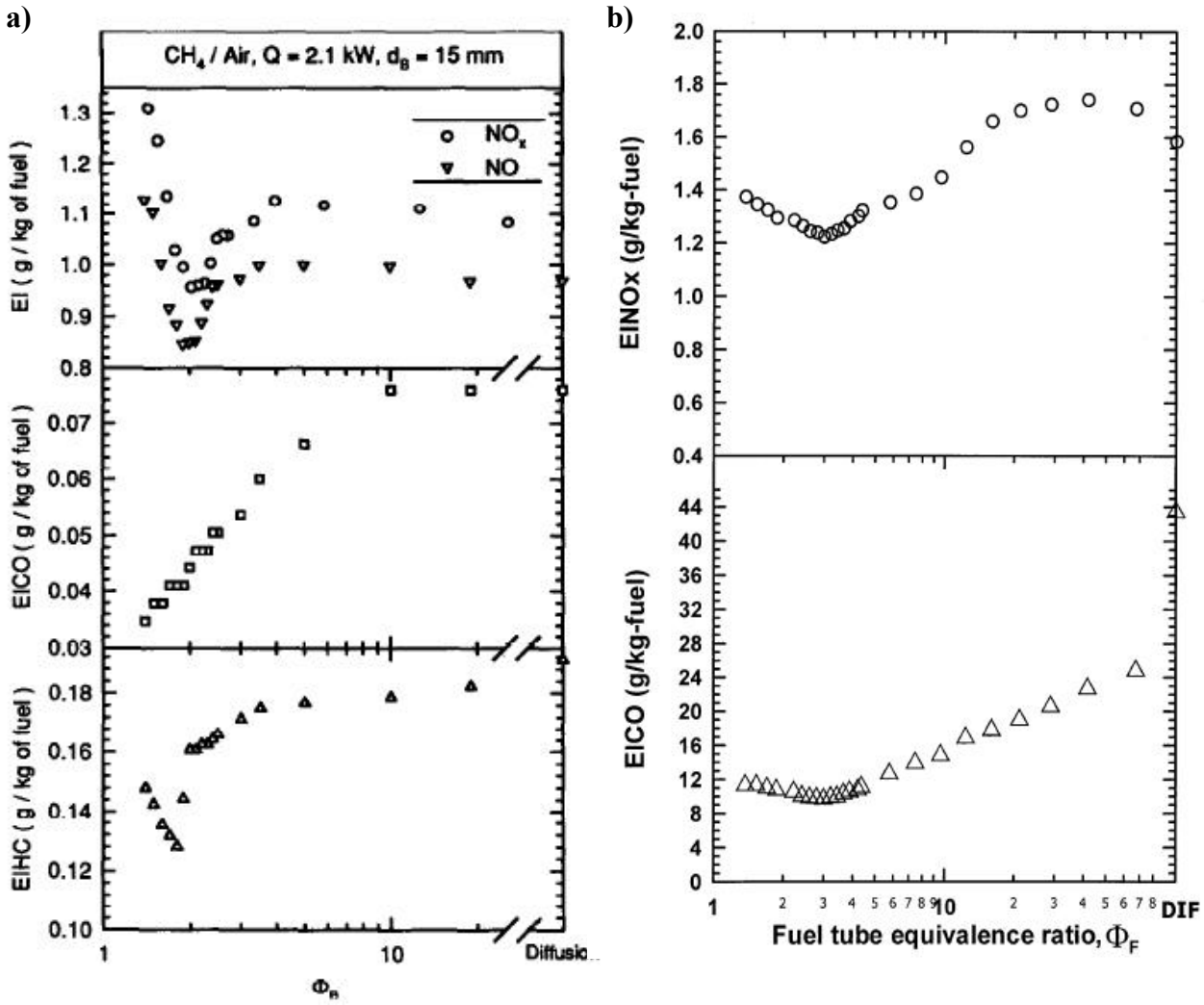

Figure 5: Emission index for NO, NO_x, CO and hydrocarbons (HC) plotted as a function of ϕ_{local} from: a) Gore and Zhan [12] and b) Cheng et al. [11], with methane as fuel

In Stefan Dittrich's master thesis, some of the same patterns as Gore et al. and Cheng et al. reported can be observed. Dittrich performed experiments with different diluents to see what effect they had on the NO_x emissions [15]. As we can see from Figure 6, premixing of air-fuel have little effect for low diluent-to-fuel ratios (DFR [mass basis]) compared with pure N_2 as diluent. But as the DFR exceeds the value one, a larger decrease in the NO_x emissions is observable. The explanation of this behavior is, according to Dittrich, that for low DFR the oxygen in the air supports the NO_x formation while the rest of the gas act as diluent and cool down the flame temperature. Both effects counteract each other, and therefore the NO_x emissions decrease much slower than for pure N_2. At high DFR the oxygen can not really support the NO_x formation anymore due to the low temperature and thus the NO_x emissions decrease faster. It should be added that these experiments were performed with a fixed fuel flow, i.e. constant effect, and a fixed flow of combustion air and subsequently an increasing amount of diluent air was added to the fuel. This will give an increase in excess air.

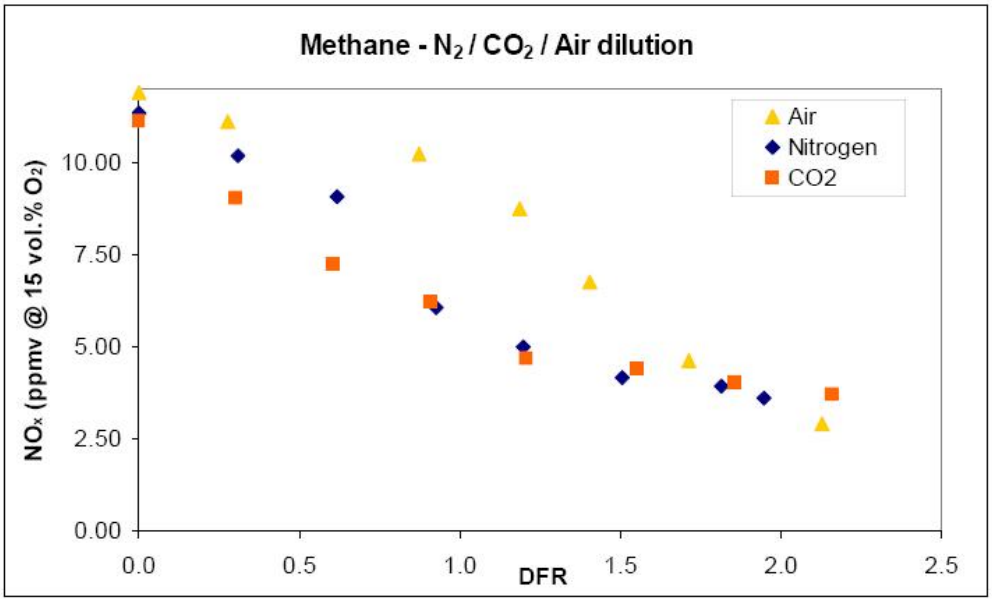

Figure 6: NO_x emissions for methane with air, N_2 or CO_2 as diluent [15]

The premixed fuel-air mixture can be highly combustible, and might cause flashbacks in the burner. It is therefore important that the mixture is above the upper flammability limit or bellow the lower flammability. The flammability limits for methane and propane is given in chapter 2.3. For propane the equivalence ratio, ϕ_{local}, has to be above 2.68 or below 0.51 to be certain that flashbacks not will occur.

2.2.3 Flue gas recirculation

Adding inert gas to the flame zone in combustion can lower the overall flame temperature. The inert gas will require heat from the combustion process, and therefore lower the overall combustion temperature. There are several examples of gases used as diluents, for instance CO_2, steam, N_2, H_2 and flue gas [3, 15-17]. The diluent of particular interest in this thesis is flue gas. Flue gas recirculation has not only the effect that it lowers the temperature, but it also reduces the O_2 partial pressure which will decrease the NO_x formation via the Zeldovich mechanism. There are in principal two ways of flue gas recirculation (FGR); internal and external FGR. In external FGR (Figure 7), flue gas is extracted from the combustor outlet, and introduced to the combustion air by an external pipe.

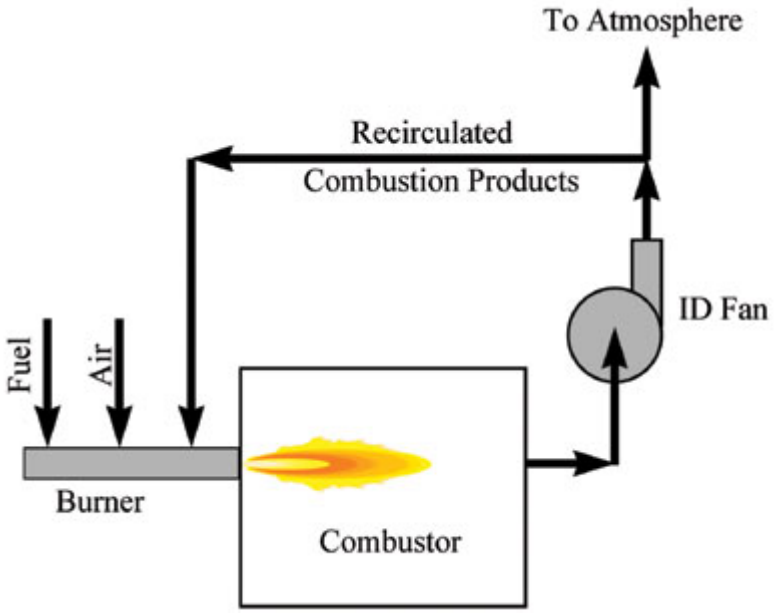

Figure 7: External flue gas recirculation system [18]

In internal FGR, the fuel gas is recycled into the flame zone due to burner aerodynamics. There are three main ways of creating internal recycling by burner adjustments; confined jets (Figure 8), confined jets with swirl (Figure 9) and flow past bluff bodies (Figure 10).

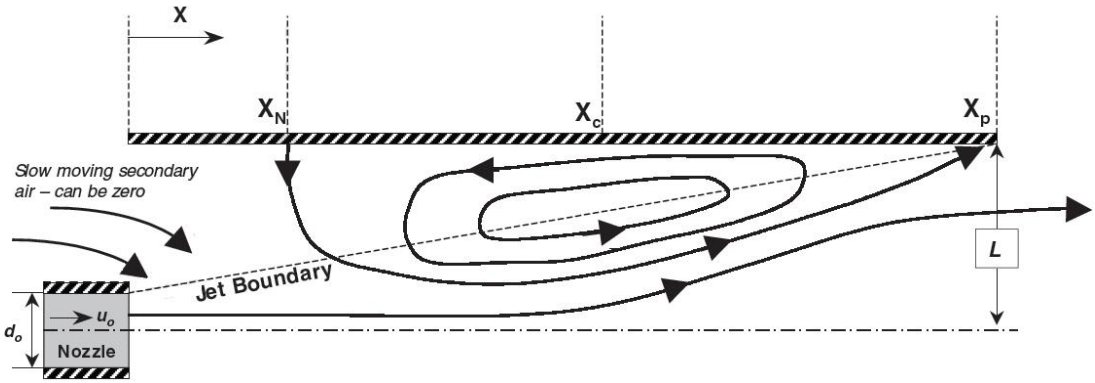

Figure 8: Axial confined jet and secondary recirculation [9]

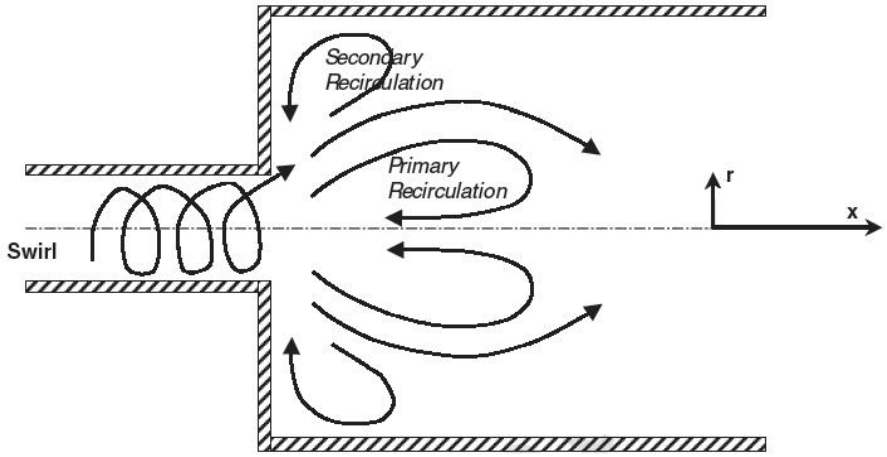

Figure 9: Creation of a central toroidal recirculation zone resulting from swirl [9]

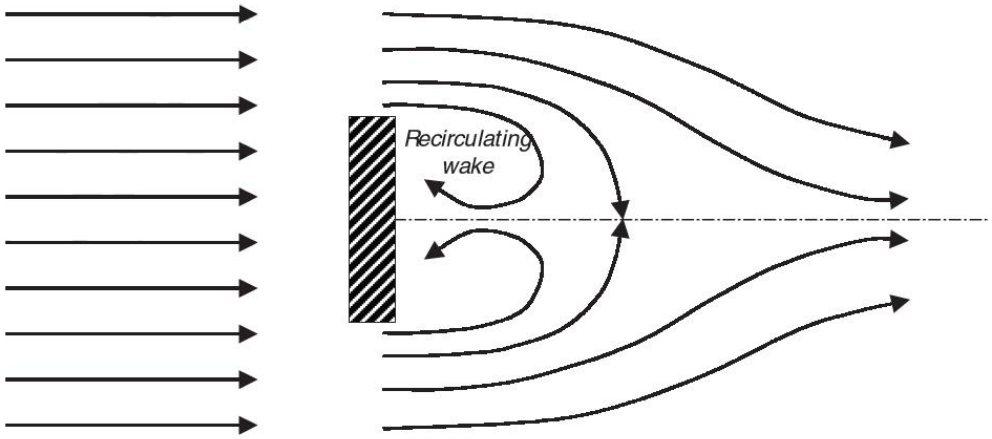

Figure 10: Recirculation caused by wake behind a bluff body [9]

The principal of all these internal FGRs is to utilize the pressure difference set up by high velocity gas streams. The burner described more closely in the experimental part of this report has a swirl generator mounted at its exit. The swirl generator will cause a radial pressure gradient given by the centrifugal force [9]:

$$\frac{dP}{dr} = \rho \frac{v_\theta^2}{r} \tag{2-13}$$

As the swirl dissipates, the pressure increases along the axial line. This contrary pressure gradient will create a backflow, referred to as central toroidal recirculation zone (CTRZ). The degree of swirl usually is characterized by a swirl number *S*, given by [9]:

$$S = \frac{G_\theta}{G_x r} = \frac{\left[\int_0^r \rho v_x v_\theta r dr\right]}{\left[\int_0^r \rho v_x v_x r dr\right] r} \tag{2-14}$$

Where G_θ is the axial flux of swirl momentum, G_x is the axial flux of the axial momentum and *r* is a characteristic radius such as the burner radius or the swirler radius. Typical profiles of axial and swirl velocity for a strong swirling flow (*S*>0.6) are shown in Figure 11

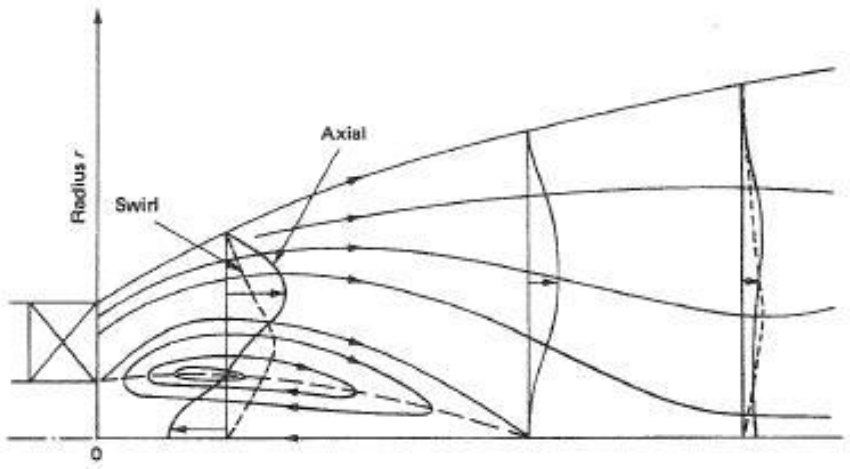

Figure 11: Flow recirculation in a strong swirling flow [3]

2.2.4 Catalytic combustion

The recent years catalytic combustion has proven to be one of the most promising NO_x reducing techniques (see Figure 12). In catalytic combustion the fuel energy is converted into heat at a lower temperature than in ordinary combustion, thus reducing production of thermal NO_x. In these systems the fuel reacts on the surface of the catalyst by a heterogeneous mechanism, where the catalyst is a ceramic or metal structure coated with noble metals. Because of the durability of the catalyst it is important to combust ultra-lean fuel-air mixtures with adiabatic combustion temperature below 1500 ˚C [19]. However, the observed reduction in NO_x in catalytic combustors is much greater than that expected from the lower combustion temperature. The reaction on the catalytic surface apparently produces no NO_x directly, although some NO_x may be produced by homogeneous reactions in the gas phase initiated by the catalyst [19].

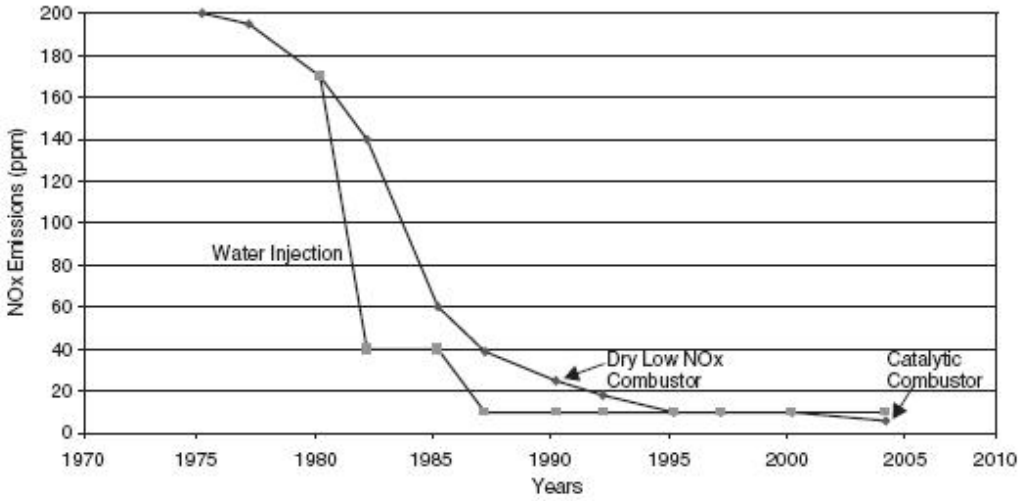

Figure 12: Control of gas turbine NO_x emission over the years [19]

2.3 Comparison of methane and propane as fuels

The most common used fuel in gas turbines is natural gas, which has methane, ethane, propane and butane as its elements. In laboratories it is common to simplify this into pure methane, the main component of natural gas. However, experiments with the actual burner modeled in this thesis failed using methane as fuel because of blow off and stability problems [3]. Because of this problem propane had to be used instead of methane, and therefore it would be necessary to compare the two fuels by having a look at their properties and the combustion process itself.

Table 1: Chemical properties of methane and propane

Gas	Chemical formula	ρ (kg/m^3)	MW [20] (kg/kmol)	LHV [20] (MJ/kg)	T_{ad} [4] (˚C)	UFL [9] (vol%)	LFL [9] (vol%)	$(FAR)_{st}$
Methane	CH_4	0.717	16.043	50.02	1953	15.0	5.0	0.0581
Propane	C_3H_8	1.809	44.370	46.36	1994	10.1	2.1	0.0639

ρ	Density at standard temperature and pressure
MW	Molecular weight
LHV	Lower heating value
T_{ad}	Adiabatic flame temperature for stoichiometric fuel to air ratio
UFL	Upper flammability limit at standard temperature and pressure
LFL	Lower flammability limit at standard temperature and pressure
$(FAR)_{st}$	Stoichiometric fuel to air ratio $(kg_{fuel}/kg_{air})_{st}$

In Table 1 the chemical properties of methane and propane are given. Propane is a heavier hydrocarbon than methane and, in contrast to methane, heavier than air. The adiabatic temperature for the two hydrocarbons is nearly the same, and only about 41 °C higher for propane. For Propane the flammability limits are shifted a bit downwards and the flammable area are smaller than for methane.

The $(FAR)_{st}$ is calculated by setting up a chemical equation with stoichiometric conditions to find the molar ratio of fuel and air. The air composition is simplified to only contain oxygen and nitrogen. The equations for methane and propane will then be as following:

$$CH_4 + 2\left(O_2 + 3.76N_2\right) \rightarrow CO_2 + 2H_2O + 7.52N_2 \tag{2-15}$$

$$C_3H_8 + 5\left(O_2 + 3.76N_2\right) \rightarrow 3CO_2 + 4H_2O + 18.8N_2 \tag{2-16}$$

These two equations tells us that for one mole of fuel, 9.52 and 23.8 mole of air is needed to achieve stoichiometric conditions for respectively methane and propane as fuels. The stoichiometric fuel air ratio can then be calculated by solving equation (2-17):

$$\left(FAR\right)_{st} = \frac{m_{fuel}}{m_{air}} = \frac{MW_{fuel}n_{fuel}}{MW_{air}n_{air}} \tag{2-17}$$

The $(FAR)_{st}$ given in Table 1 shows us that for the same amount of fuel burned, a little more air is needed to get a complete combustion of the methane. The difference is so little that it does not need to be considered when designing the burner. The $(FAR)_{st}$ can be used as a reference when describing if a mixture of fuel and air is rich or lean. This is called the equivalence ratio ϕ, and can be defined as:

$$\phi = \frac{\left(FAR\right)}{\left(FAR\right)_{st}} = \frac{1}{\lambda} \tag{2-18}$$

Where $\phi \approx \infty$ describes a diffusion flame, $\phi > 1$ is a rich mixture, $\phi < 1$ is a lean mixture and $\phi = 1$ stoichiometric conditions.

When it comes to the NO_x emission of the two fuels, there are some major differences. Experiments with methane and propane performed by Spangelo showed a difference in NO_x emissions of about 1.5 or 2 times depending on the power output [3]. The results from these experiments are given in Figure 13.

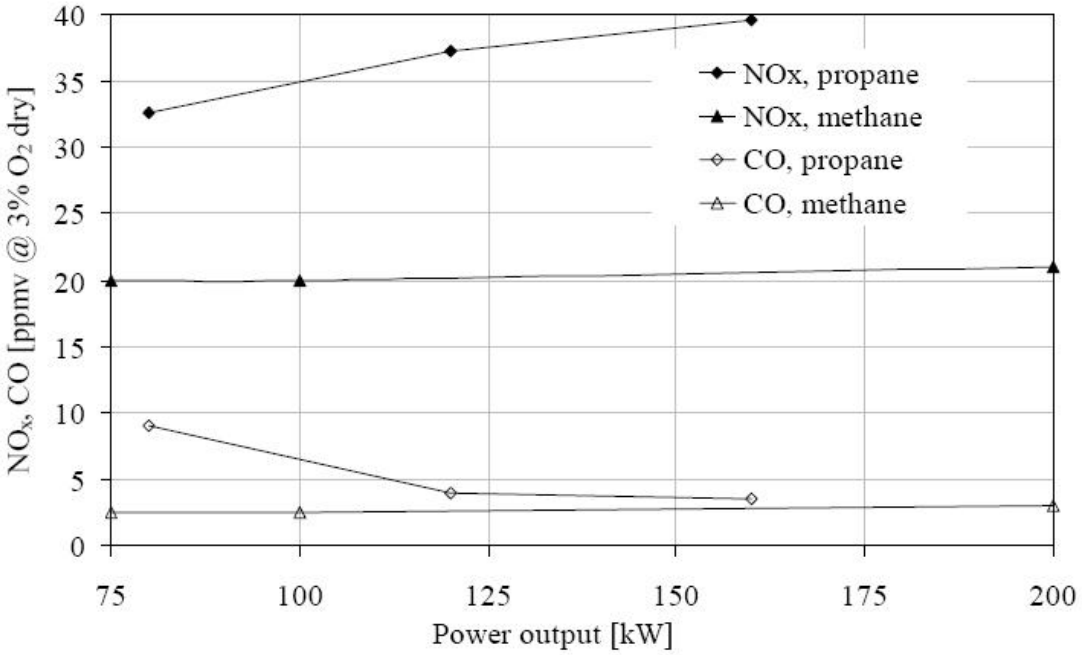

Figure 13: NO_x and CO emissions as a function of power output and fuel, swirl number: S=2,7 [3]

The reason for the increase in emissions of nitrogen oxides when burning propane versus methane is due to the prompt mechanism which is less significant for methane as fuel and more significant for higher hydrocarbons [21]. When burning higher hydrocarbons, like propane, the concentration of hydrocarbon radicals increases and therefore the formation of NO_x through the prompt mechanism also increase.

The effect of partial premixing on NO_x emissions is strongly dependent on the fuel. This can be seen from the experiments performed by Turns et al. plotted in Figure 14 [10]. As mentioned in chapter 2.2.2, the NO_x emissions for methane is lower for higher premixing rations than for a diffusion flame. For propane a much higher increase in the NO_x emissions are observed, reaching a peak in the emissions at $\phi_{local} \approx 10$. Further increase in the level of premixing will give a decrease in the NO_x emissions, but not below the emission from the diffusion flame. However, the experiments using propane as fuel were not performed for ratios below approximately $\phi_{local} = 4.75$ and therefore no further conclusion about the NO_x emissions can be made for equivalence ratios below this. Also seen from Figure 14 is the rise in temperature for higher premixing ratios. This is explained by Turns et al. as a consequence of the countervailing influence of suppressed soot formation, which tends to make the flames more adiabatic [10].

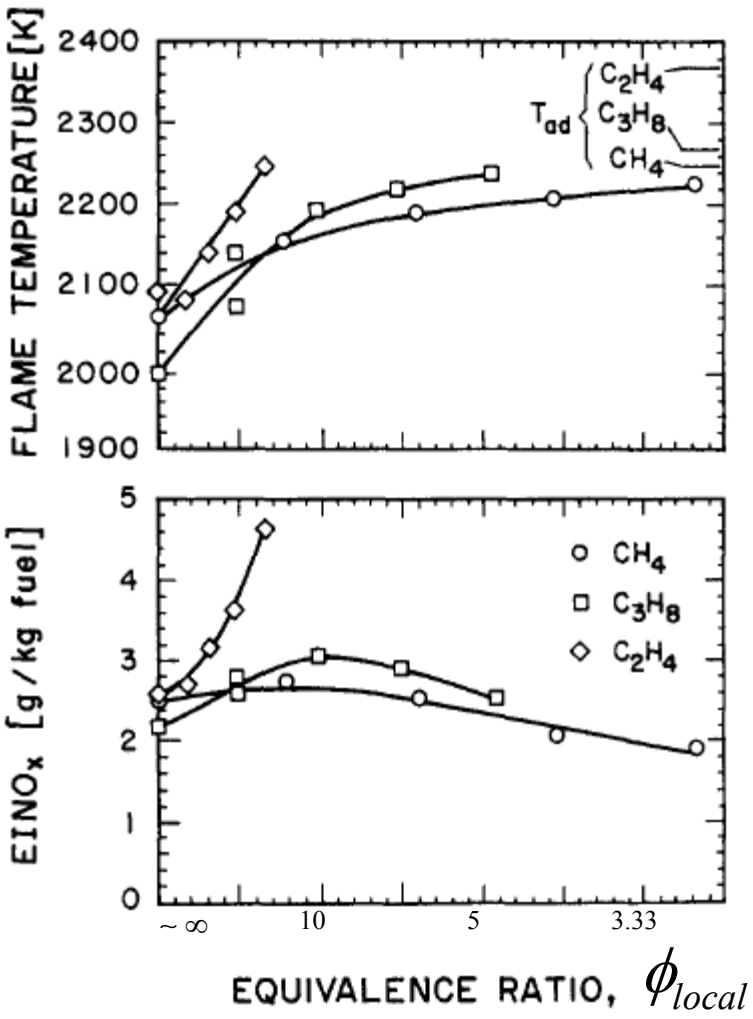

Figure 14: Effects of partial premixing on flame temperatures and NO_x emission indices for different fuels [10]

2.4 Computational fluid dynamic

Applying the fundamental laws of mechanics to a fluid gives the governing equations for a fluid. These equations form a set of coupled nonlinear partial differential equations, which for most practical engineering problems is not solvable analytically. However there is possible to get an approximate solution by using computer-based numerical methods to solve the governing equations. This is the main objective of using computational fluid dynamics (CFD).

2.4.1 Governing equations of fluid flow and heat transfer

In this section the conservation equations for mass, species mass, momentum and energy will be briefly discussed.

Conservation of mass
The continuity equation describes the convective transport and change of the total mass in an infinitesimal volume $V = dxdydz$. The continuity equation is derived from the conservation law that states that the net rate at which mass enters the control volume must equal zero [22]. Equation (2-19) gives the differential form of the continuity equation:

$$\frac{\partial \rho}{\partial t} + \frac{\partial}{\partial x_j}\left(\rho u_j\right) = 0 \tag{2-19}$$

Where ρ is the density and u_j is the Cartesian velocity component in the x_j-direction.

If the fluid is a mixture of different species *k* in the same phase, an equation for each of the species of local mass fraction $Y_k = \frac{m_k}{m_{tot}}$ can be written on the form:

$$\frac{\partial}{\partial t}\left(\rho Y_k\right) + \frac{\partial}{\partial x_j}\left(\rho Y_k u_j\right) = \frac{\partial}{\partial x_j}\left(-j_{k,j}\right) + R_k \tag{2-20}$$

Where R_k is the production rate of species *k* by chemical reaction and $J_{n,i}$ is the diffusion flux of species *k* which arises due to gradients in the species concentration. The diffusion flux can be modeled by using Fick's law:

$$-J_{k,i} = \rho D_k \frac{\partial Y_k}{\partial x_i} \tag{2-21}$$

where D_k is the diffusion coefficient for species *k* in the mixture.

Conservation of momentum
The conservation of momentum derives from Newton's second law of motion, which states that the sum of all forces acting on the control volume must equal the net rate at which momentum leaves the control volume [22]. The equation for an incompressible fluid in the *i*-direction can be written as follows:

$$\frac{\partial}{\partial t}\left(\rho u_i\right) + \frac{\partial}{\partial x_j}\left(\rho u_i u_j\right) = \frac{\partial p}{\partial x_i} + \frac{\partial \tau_{ij}}{\partial x_j} + \rho f_i \tag{2-22}$$

Where *p* is the static pressure and ρf_i is an external body force like gravity or electromagnetic forces.

The stress tensor τ_{ij} is given by equation (2-23):

$$\tau_{ij} = \mu\left(\frac{\partial u_i}{\partial x_j} + \frac{\partial u_j}{\partial x_i}\right) + \left(\mu_b - \frac{2}{3}\mu\frac{\partial u_k}{\partial x_k}\delta_{ij}\right) \tag{2-23}$$

Where μ is the molecular viscosity and μ_b is the bulk viscosity. An common assumption, referred to as the Stokes hypothesis, is to set the bulk viscosity $\mu_b = 0$ [23].

Conservation of energy
The law of conservation of energy states that the total amount of energy in any isolated system remains constant but cannot be recreated, although it may change forms, e.g. friction turns kinetic energy into thermal energy. The conservation of energy can be described by equation (2-24) [23]:

$$\frac{\partial}{\partial t}(\rho h) + \frac{\partial}{\partial x_j}(\rho h u_j) = \frac{\partial}{\partial x_j}\left(\rho\alpha\frac{\partial h}{\partial x_j}\right) + S_h \tag{2-24}$$

Where $\alpha = \dfrac{\lambda}{\rho C_p}$ is the thermal viscosity. This way of describing the conservation energy assumes ideal gas or constant pressure, such that $h = h(T)$. Fourier's Law of heat conduction contains temperature gradients, not enthalpy gradients, so some simplifications are required. The content of the source term, S_k, depends on what simplifications that is made.

For further reading about the governing equations of fluid flow and heat transfer, fundamental books written by Incropera & DeWitt [22], Ertesvåg [23] and White [24] is recommended.

2.4.2 Generalized conservation equation

The different conservation equations described in the preceding chapter, (2-20), (2-22) and (2-24) can be generalized to an equation for an arbitrary scalar φ:

$$\underbrace{\frac{\partial}{\partial t}(\rho\varphi)}_{\text{transient term}} + \underbrace{\frac{\partial}{\partial x_j}(\rho\varphi u_j)}_{\text{convective term}} = \underbrace{\frac{\partial}{\partial x_j}\left(\Gamma_\varphi\frac{\partial\varphi}{\partial x_j}\right)}_{\text{diffusive term}} + \underbrace{S_\varphi}_{\text{source term}} \tag{2-25}$$

2.4.3 Computation of turbulent flow

Turbulence is an extremely complicated subject and considerable effort has been made over the years to understand turbulence and develop methods that can model turbulent flow [4]. The essential problem of solving a turbulent flow is all the information necessary to describe the flow and modeling may result in large errors, especially for flow conditions that have not been studied experimentally. In this chapter, some basic background on how turbulent flow can be described mathematically will be given in addition with a description of the turbulent models that will be used and referred to in this thesis.

Turbulent flow results when fluctuations in the flow are not sufficiently damped by viscous action and the fluid velocity at each point in the flow exhibits random fluctuations [4]. One way of describing turbulent flow, is to split the fluid properties into a mean and fluctuating quantity (Reynolds decomposition):

$$\varphi = \overline{\varphi} + \varphi' \tag{2-26}$$

How the mean properties are defined, varies. For instance a time-average, a sample-median or a probability density function (PDF) can be used [23]:

Time-average:
$$\overline{\varphi} = \frac{1}{\Delta t}\int_{t-\frac{1}{2}\Delta t}^{t+\frac{1}{2}\Delta t} \varphi(t)dt \tag{2-27}$$

Sample-median:
$$\overline{\varphi} = \frac{1}{N}\sum_{n=1}^{N}\varphi_n \tag{2-28}$$

PDF:
$$\overline{\varphi} = \int_{-\infty}^{\infty} \varphi(c) f(c)\, dc \tag{2-29}$$

With the use of Reynolds decomposition and the assumption that ρ is constant, the governing equations can be written on the form [23]:

Continuity:
$$\frac{\partial \overline{u}_j}{\partial x_j} = 0 \text{ and } \frac{\partial u'_j}{\partial x_j} = 0 \tag{2-30}$$

Momentum:
$$\frac{\partial}{\partial t}\left(\rho\overline{u}_i\right) + \frac{\partial}{\partial x_j}\left(\rho\overline{u}_i\overline{u}_j\right) = -\frac{\partial \overline{p}}{\partial x_i} + \left(\overline{\tau}_{ij} - \rho\overline{u'_i u'_j}\right) + \rho\overline{f_i} \tag{2-31}$$

Mass fraction:
$$\frac{\partial}{\partial t}\left(\rho\overline{Y_k}\right) + \frac{\partial}{\partial x_j}\left(\rho\overline{Y_k}\overline{u}_j\right) = \frac{\partial}{\partial x_j}\left(\rho D\frac{\partial \overline{Y_k}}{\partial x_j} - \rho\overline{Y'_k u'_j}\right) + \overline{R_k} \tag{2-32}$$

Energy:
$$\frac{\partial}{\partial t}\left(\rho\overline{h}\right) + \frac{\partial}{\partial x_j}\left(\rho\overline{h}\overline{u}_j\right) = \frac{\partial}{\partial x_j}\left(\rho\alpha\frac{\partial \overline{h}}{\partial x_j} - \rho\overline{h'u'_j}\right) + \overline{S_h} \tag{2-33}$$

The equations (2-30), (2-31), (2-32) and (2-33) are referred to as the Reynolds averaged equations, or the Reynolds equations. These are equations for the averaged fluid properties, and can be solved numerical. The problem, in addition to the source terms, is that new unknown variables, $-\rho\overline{u_i'u_j'}$, $-\rho\overline{Y_k'u_j'}$ and $-\rho\overline{h'u_j'}$, arises. These terms are referred to as Reynolds flux and stress terms. The terms are a problem because the number of unknowns is now being higher than the number of equations to solve. This problem is known as the closure problem and can only be resolved by adopting some kind of model to represent the Reynolds flux and stress terms.

In CFD software the models are divided into two basic levels [3], The first-order Eddy Viscosity/Diffusivity Models and the second-order Reynolds Stress Models. There exist several variants of these models, and further literature studies are recommended. In this thesis two different first-order models, the standard k-ε model and the RNG k-ε model, and a second order Reynolds stress model are used and referred to. Therefore this report only describes these three models in the following.

2.4.3.1 The standard k-ε model

The standard k-ε model is a semi-empirical model, and the derivation of the model equations relies on phenomenological considerations and empiricism. The model has proven itself to be a robust, economical and reasonable for a wide range of turbulent flows and is therefore popular in industrial simulations. The Eddy Viscosity/Diffusivity Models are based on the assumption that the Reynolds Stress terms can be related to the mean velocity gradients by using a turbulent/eddy viscosity (μ_t) as in the following expression [3]:

$$-\rho\overline{u_i'u_j'} = \mu_t\left(\frac{\partial\overline{u}_i}{\partial x_j}+\frac{\partial\overline{u}_j}{\partial x_i}\right)-\frac{2}{3}\left(\rho k+\mu_t\frac{\partial\overline{u}_i}{\partial x_i}\right)\delta_{ij} \tag{2-34}$$

Where k is the turbulent kinetic energy [23]:

$$k=\frac{1}{2}\overline{u_i'u_i'} \tag{2-35}$$

The dissipation ε can be expressed as [23]:

$$\varepsilon = C_D\frac{k^{3/2}}{L} \tag{2-36}$$

Where L is a length scale for the larger eddies. With the use of equation (2-36) and an analogy to the model of molecular viscosity, a model of the turbulent viscosity can be derived:

$$\mu_t = \rho C_\mu \frac{k^2}{\varepsilon} \tag{2-37}$$

With the use of the equations (2-22), (2-26), (2-34), (2-35) and (2-37) two transport equations, one for turbulent kinetic energy and one for its dissipation, can be expressed [23]:

$$\frac{\partial}{\partial t}(\rho k) + \frac{\partial}{\partial x_j}\left(\rho k \overline{u}_j\right) = \frac{\partial}{\partial x_j}\left[\left(\mu + \frac{\mu_t}{\sigma_k}\right)\frac{\partial k}{\partial x_j}\right] + \rho P_k - \rho\varepsilon \tag{2-38}$$

$$\frac{\partial}{\partial t}(\rho \varepsilon) + \frac{\partial}{\partial x_j}\left(\rho \varepsilon \overline{u}_j\right) = \frac{\partial}{\partial x_j}\left[\left(\mu + \frac{\mu_t}{\sigma_\varepsilon}\right)\frac{\partial \varepsilon}{\partial x_j}\right] + C_{\varepsilon 1}\frac{\varepsilon}{k}\rho P_k - C_{\varepsilon 2}\frac{\varepsilon}{k}\rho\varepsilon \tag{2-39}$$

where ρP_k represents the generation of turbulence kinetic energy due to the mean velocity gradients. The constants C_μ, $C_{\varepsilon 1}$, $C_{\varepsilon 2}$, σ_k and σ_ε are found empirically, and values found by Launder and Spalding in 1974 is still widely used [23]. The constants are listed in Table 2.

Table 2: Constants in the standard k-ε model [3]

C_μ	$C_{\varepsilon 1}$	$C_{\varepsilon 2}$	σ_k	σ_ε
0.09	1.44	1.92	1.00	1.30

The same method can be used to model the Reynolds fluxes, se reference [23] for details.

The standard k-ε model has some problems representing the following effects[23]:

- Strong streamline curvature
- Strong anisotropy in the Reynolds Stress terms
- External forces working on the fluid, which are dependent on the direction. E. g. buoyancy and Coriolis forces
- If the turbulence production has large variances from equilibrium

Despite these drawbacks the standard k-ε model has proven to perform satisfactory in most cases, and can in any case give a quick and rough calculation of the flow field [3].

2.4.3.2 The Renormalized (RNG) k-ε model

The RNG k-ε model was derived using a rigorous statistical technique (called renormalization group theory). It is similar in form to the standard k-ε model, but includes the following refinements [6]:

- The RNG model has an additional term in its ε-equation that significantly improves the accuracy for rapidly strained flows
- The effect of swirl on turbulence is included in the RNG model, enhancing accuracy for swirling flows

- The RNG theory provides an analytical formula for turbulent Prandtl numbers, while the standard k-ε model uses user-specified, constant values
- While the standard k-ε model is a high-Reynolds-number model, the RNG theory provides an analytically-derived differential formula for effective viscosity that accounts for low-Reynolds-number effects. Effective use of this feature does, however, depend on an appropriate treatment of the near-wall region

There are quite a few mathematical operations and assumptions that lies behind these refinements, and to go deeply in to them will be to comprehensive for this thesis. Further details about the RNG k-ε model can be found in the literature [6, 23].

2.4.3.3 The Reynolds Stress Model (RSM)

In the same way as for the *k*-equation (2-38), the equation for the Reynolds stresses can be derivated from the governing equations. The exact transport equations for the transport of the Reynolds stresses, $\rho\overline{u_i'u_j'}$, may be written as follows (constant density) [23]:

$$\underbrace{\frac{\partial}{\partial t}\left(\rho\overline{u_i'u_j'}\right)+\frac{\partial}{\partial x_k}\left(\rho\overline{u_i'u_j'}\overline{u}_k\right)}_{\rho C_{ij}}=\underbrace{-\left(\rho\overline{u_i'u_k'}\frac{\partial\overline{u}_j}{\partial x_k}+\rho\overline{u_j'u_k'}\frac{\partial\overline{u}_i}{\partial x_k}\right)}_{\rho P_{ij}}+\underbrace{\frac{\partial}{\partial x_k}\left(\mu\frac{\partial\overline{u_i'u_j'}}{\partial x_k}\right)}_{\rho D_{ij,v}}$$
$$+\underbrace{\frac{\partial}{\partial x_k}\left(-\rho\overline{u_i'u_j'u_k'}-\left(\overline{p'u_i'}\delta_{jk}+\overline{p'u_j'}\delta_{ik}\right)\right)}_{\rho D_{ij,t}} \qquad (2\text{-}40)$$
$$+\underbrace{\overline{p'\left(\frac{\partial u_i'}{\partial x_j}+\frac{\partial u_j'}{\partial x_i}\right)}}_{\rho\Phi_{ij}}-\underbrace{2\mu\overline{\frac{\partial u_i'}{\partial x_k}\frac{\partial u_j'}{\partial x_k}}}_{\rho\varepsilon_{ij}}$$

Where C_{ij} is transient and convective transportation with the mean flow; P_{ij} is stress production, transport of mechanical energy from the mean flow to the turbulence; $D_{ij,v}$ and $D_{ij,t}$ is respectively the viscous and turbulent diffusion; Φ_{ij} is the redistribution or exchange of energy between the components (pressure-strain term); and ε_{ij} is the dissipation, transmission from kinetic to thermal energy.

The terms C_{ij}, P_{ij} and $D_{ij,v}$ does not require any modeling. However the rest of the terms need to be modeled to close the equations. The following sections describe the modeling assumptions required to close the equation set.

The turbulent diffusion, $D_{ij,t}$, can be modeled by the generalized gradient-diffusion model of Daly and Harlow [23]:

$$D_{ij,t} = \frac{\partial}{\partial x_k}\left(C_s \frac{k}{\varepsilon} \overline{u_k' u_l'} \frac{\partial \overline{u_i' u_j'}}{\partial x_l} \right) \tag{2-41}$$

However, equation (2-41) can result in numerical instabilities, and is therefore often simplified to use a scalar turbulent diffusivity as follows [6]:

$$D_{ij,t} = \frac{\partial}{\partial x_k}\left(\frac{\mu_t}{\sigma_k} \frac{\partial \overline{u_i' u_j'}}{\partial x_k} \right) \tag{2-42}$$

Where the turbulent viscosity, μ_t, can be computed using equation (2-37). The value of the constant σ_k varies. For instances Lien and Leschziner value of $\sigma_k = 0.82$ can be used [6].

The most common way of describing the dissipation term, ε_{ij}, is to use an isotropic model [23]:

$$\varepsilon_{ij} = \frac{2}{3}\varepsilon\delta_{ij} \tag{2-43}$$

Where equation (2-39) can be used to model the turbulence dissipation rate, ε.

The pressure-strain term, Φ_{ij}, can be model with the use of Rotta's theory [23]:

$$\Phi_{ij} = -C_1 \frac{\varepsilon}{k}\left(\overline{u_i' u_j'} - \frac{2}{3} k\delta_{ij} \right) - C_2 \left(P_{ij} - \frac{1}{3} P_{kk}\delta_{ij} \right) \tag{2-44}$$

Different values are used for the constants C_1 and C_2. There exist other models that describe the pressure-strain term, all of them with both negative and positive effects when solving the Reynolds Stress Model [23].

2.4.4 Modeling of swirl flow

The assumption in the standard k-ε model and the RNG k-ε model that the turbulence is isentropic is not applicable when modeling swirling flows. Other inadequacies of the two first-order equations are the lack of possibilities to account for extra strain and the poor prediction of flows with large pressure gradients [3].

However, some workers have succeed to predict strong swirling flows ($S > 0.5$) using the first-order models. For instance, Frassoldati et al. managed to predict the turbulent mixing zone within the experimental results with the use of the standard k-ε model [25]. Nevertheless, in the literature, the use of first-order models is not recommended [3, 6].

2.4.5 Modeling reacting flow

When introducing chemical species reactions in addition to the flow, the problem is further complicated. Every global reaction mechanisms might consist of hundreds or even thousands of elementary reactions, and modeling detailed chemistry demands large computer resources. Because of the complexity, simplifying assumptions has to be made. The following sections will give a description of the reacting flow models referred to in this thesis, the eddy dissipation model, the equilibrium model and the flamelet model.

2.4.5.1 The eddy dissipation model

The assumption of this model is that the chemical reactions are infinitely fast, and that the reaction rate therefore is controlled by the turbulent mixing [23]. The difference between the eddy dissipation model and other eddy models is that the chemical reaction is said to be controlled by the species that has the smallest local concentration. The reaction rate can be modeled by equation (2-45), where $\overline{Y}_f$, $\overline{Y}_o$ and $\overline{Y}_p$ are local mean mass fractions of fuel, oxidizer and products respectively [23]:

$$\overline{R}_f = A\rho\frac{\varepsilon}{k}\min\left(\overline{Y}_f, \frac{1}{v}\overline{Y}_o, B\frac{1}{1+v}\overline{Y}_p\right) \tag{2-45}$$

A and B are empirical constants and v is the stoichiometric oxidizer to fuel mass ratio.

2.4.5.2 Equilibrium and flamelet mixture fraction model

The eddy dissipation model, models the transport and source term for mean properties like concentration or energy. A different approach is to look at the definition of the mean value and model the functions involved.

As mentioned earlier in this chapter, mean values can be written as the following:

$$\overline{G} = \int_{-\infty}^{\infty} G(\xi) f(\xi) d\xi \tag{2-46}$$

Where $f(\xi)$ is the probability density function. Every point $(\vec{x},t)$ has its own probability density, which makes $f(\xi)$ dependent of time and space. When using equation (2-46), a function relation, $G = G(\xi)$, needs to be known. Every stochastic variable G is expressed as a function of a characteristic variable ξ. The probability density function also needs to be known, and can be expressed by using a prescribed function like the β-function or Gaussian distribution found from empirical data [23].

Equilibrium and flamelet models are used for properties with source terms (non-conserved scalars). For a property π that is not conserved, the function $\pi = \pi(\xi)$ in general is not linear. The function $\pi(\xi)$ can be found by assuming equilibrium on the product side of the chemical equation (CO_2, CO, H_2O, H_2, etc), or by using predefined

connections for the different $\pi(\xi)$ (called flamelet model). In contrast to the equilibrium model, the flamelet model incorporates detailed chemical mechanisms resulting in more realistic predictions of the turbulent flow [3].

3 CFD simulations

In the following chapters a description of the burner that is modeled and the modeling process will be given. It is important to state that using CFD to model physical phenomena will not give the exact truth. Under most circumstances, property variation trends can be accurately predicted but the property quantity itself cannot be pinpointed. Accurate prediction of trends can cut down on the number of laboratory tests, allow more design variations to be studied, shorten the design cycle, and reduce product development cost. That is truly the power of CFD.

3.1 Description of the burner to be modeled

The burner modeled in this thesis is a 20 kW gas burner. It is a part of an apparatus rig standing in the laboratory at the Department of Energy and Process, consisting of fuel and air supply, burner and a combustion chamber. To the rig it is also possible to connect a diluent flow to the fuel supply. The apparatus has been widely used for experimental studies the last 10-15 years [3, 15, 21]. A schematic overview of the whole rig is given in Figure 15, and pictures of the rig and the swirl burner is attached in Appendix C.

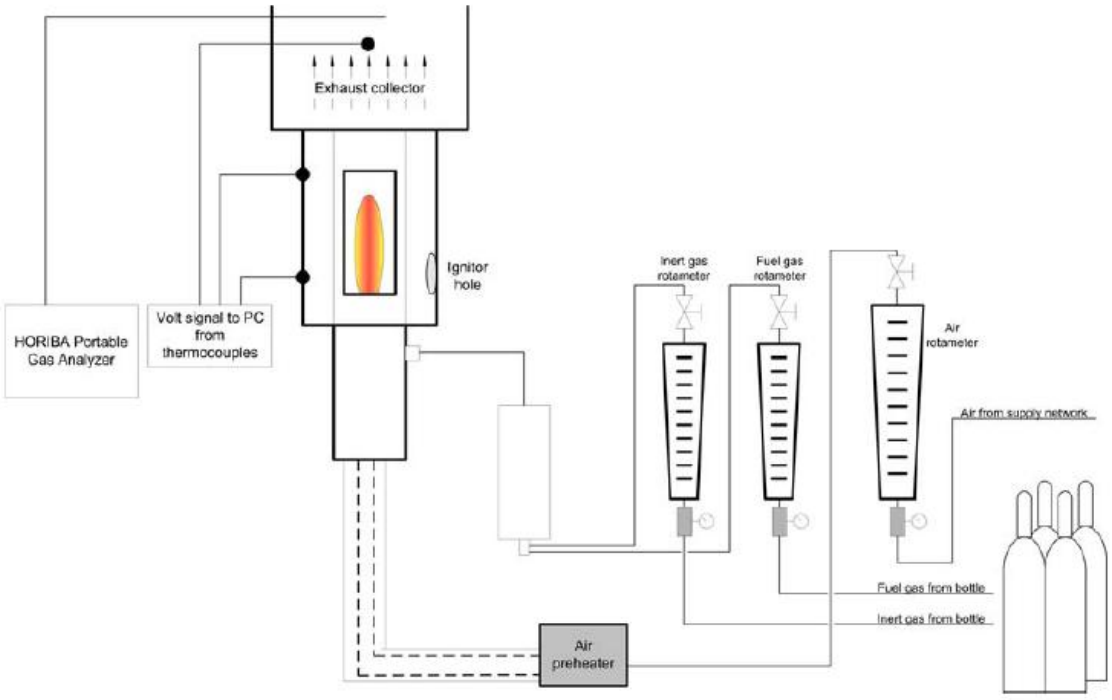

Figure 15: Schematic view of the apparatus rig [15]

The actual burner modeled in this thesis was designed by Øystein Spangelo, when working on a scaling problem of swirl burners in his Ph.D. [3]. The burner consists of an inner gas tube from where fuel gas is injected into the air flow through gas nozzles which consists of drilled holes in the gas tube. The air flows through the annulus, from now on

referred to as the burner tube, surrounding the gas tube where it is given a swirl by a vane swirl generator. The fuel air mix is then introduced into the combustion chamber by a converging conical section. The NO_x reducing technique implemented in this burner is the swirl generator. The aim of this swirl generator is to decrease the temperature and the partial pressure of oxygen by creating a central toroidal recirculation zone as described in chapter 2.2. The swirl number was set to approximately $S \approx 1.285$, calculated from equation [3]:

$$S = \frac{2}{3}\left(\frac{1-(d_h/d)^3}{1-(d_h/d)^2}\right)\tan\beta \qquad (3\text{-}1)$$

Where $d_h = 13.5mm$, $d = 34mm$ and $\beta = 60^\circ$ is as defined in Figure 16.

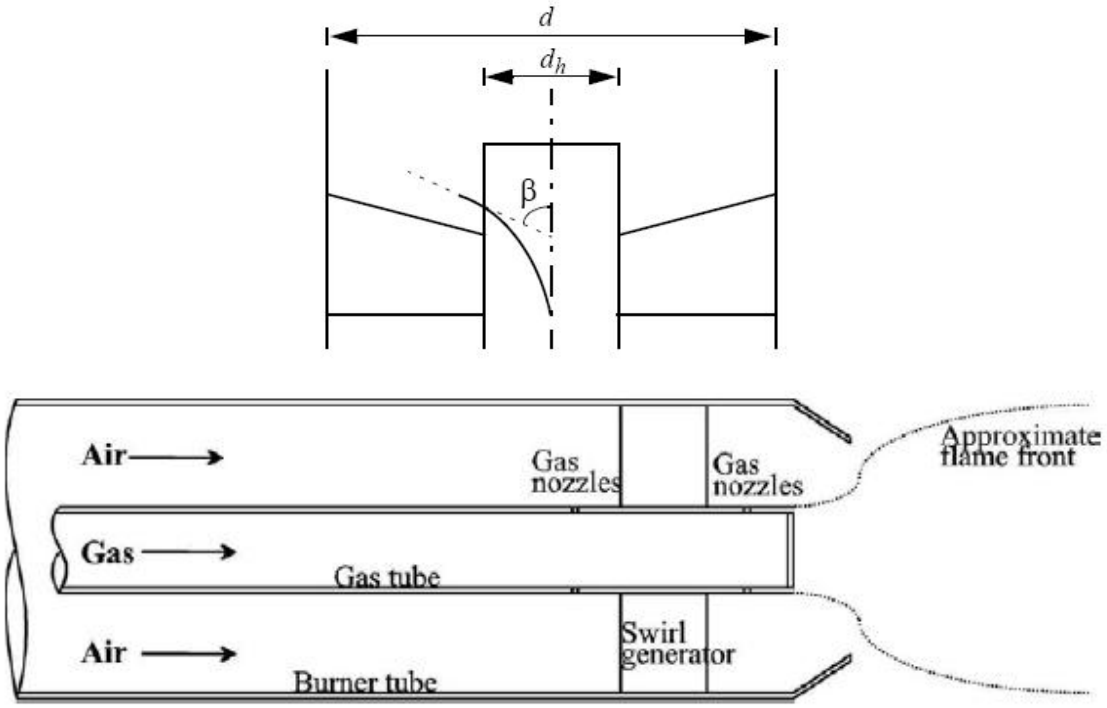

Figure 16: Diagram of the swirl burner [3]

The burner was originally designed to work in the power range of 5-20 kW, but in practice it has proven difficult to operate in that range [3]. Problems like flame stability and lift off have been observed depending on what combustion chamber that is used. In an un-cooled combustion chamber problems with instability have been observed at low flow rates of fuel and air (5-10 kW). When using a water-cooled combustion chamber, the problem with stability becomes worse. In this type of combustion chamber, lift off and subsequently blow off occurred at high flow rates using propane as fuel. With methane as fuel, the flame could not be stabilized at all. These results are of interest when deciding at what power output the burner should be modeled and simulated. The stability observations made by Øystein Spangelo are summarized in Table 3.

Table 3: Stability observations of the 20 kW swirl burner [3]

Power Output	Un-cooled Chamber		Water-cooled Chamber	
[kW]	Propane	Methane	Propane	Methane
5	Unstable	No Flame	Unstable	No Flame
10	Stable	Unstable	Stable	No Flame
15	Stable	Stable	Stable	No Flame
20	Stable	Stable	No Flame (lift off at 17 kW	No Flame

3.2 Simulation setup

The main goal of this thesis is, with the help of CFD, to investigate how the NO_x emission changes when implementing partial premixing in a gas burner. It is therefore important to establish different scenarios, and to make some assumptions about the operating conditions.

Because of the stability and lift off problems at some of the power outputs, it was decided to run simulations at a power output of 10 kW with propane as fuel to ensure that the scenario is physical possible. To minimize factors other than partial premixing that effect the NO_x emission, the excess air and the nozzle velocity were set constant. The excess air was fixed at 3 vol% O_2, and the nozzle velocity was held constant by changing the nozzle area (Denoted as A_{nozzle} in Table 4). The velocity in the burner tube is assumed to change so little that it will not affect the emissions. For more information about the constant velocity calculations see appendix A.1.

The mass flow of fuel and air with a power output of 10 kW was found by solving equations (3-2) and (3-3):

$$\dot{m}_{fuel} = \frac{P}{LHV_{fuel} \cdot 1000} = \frac{10[kW]}{46.37\left[MJ/kg\right] \cdot 1000} = \underline{\underline{0.0002156567}}\left[kg_{fuel}/s\right] \tag{3-2}$$

$$\dot{m}_{air} = \frac{\dot{m}_{fuel}}{\left(\frac{MW_{fuel}\phi}{MW_{air} n_{air,stoich}}\right)} = \frac{0.0002156567\left[kg_{fuel}/s\right]}{\left(\frac{44.37\left[kg_{fuel}/kmol_{fuel}\right] \cdot 0.87}{28.96\left[kg_{air}/kmol_{air}\right] \cdot 23.8[kmol_{air}]}\right)} = \underline{\underline{0.003891029}}\left[kg_{air}/s\right] \tag{3-3}$$

Where P is the power output, LHV_{fuel} is the lower heating value for propane given in chapter 2.3, ϕ is the overall combustion equivalence ratio and n_{air} is the amount of mole air in a stoichiometric propane-air combustion.

In collaboration with supervisor Professor Johan Hustad, it was decided to limit the amount of simulations to eight different premixed air-fuel ratios ($\frac{\dot{m}_{air}}{\dot{m}_{fuel}}$). The ratios simulated were 0, 1/2, 1, 3/2, 2, 3, 7/2 and 4. Different properties for the different air-fuel ratios are given in Table 4.

Table 4: Properties for different air-fuel ratios at 10 kW

$\dot{m}_{air} / \dot{m}_{fuel}$	$\dot{m}_{burner\ tube}$ [kg/s]	$\dot{m}_{gas\ tube}$ [kg/s]	A_{nozzle} [mm^2]	*Vol% fuel in gas tube*	ϕ_{local}
0	0.003891029	0.0002156567	39.27	100	∞
0.5	0.003762746	0.0003234850	69.149	56.6	31.1
1	0.003675372	0.0004313130	99.298	39.5	15.5
1.5	0.003567544	0.0005391420	129.448	34.3	12.4
2	0.003459716	0.0006469700	159.597	24.6	7.8
3	0.003244059	0.0008626270	219.896	17.9	5.2
3.5	0.003136231	0.0009704550	250.046	15.7	4.4
4	0.003028402	0.0010782840	280.195	14.0	3.9
5.8	0.002856726	0.0012499660	331.343	10.1	2.7

The air-fuel ratio of 5.8 is the highest possible ratio before reaching the upper flammability limit and is included here for comparison. In practice this air-fuel ratio is too dangerous to operate at with a view to flash back and explosion risk.

3.3 Implementation of CFD

The modeling of the burner was carried out by using the CFD software FLUENT. FLUENT is a commercial computer program for modeling fluid flow and heat transfer in complex geometries, and the code is programmed in a C-language. The governing equations are solved by means of iterations with the help of the models described in chapter 2.4.

There exist several other commercial CFD programs on the market, for instance KFX, CFX, Comsol Multiphysics, PHOENICS and CFD-ACE. The reason why FLUENT was chosen as the modelling tool was because of the previous work done by Øystein Spangelo [3]. The modelling, simulations and verification against experimental data in Spangelo's Ph.D. made it possible to model the partially premixed swirl burner within the time limit of this master thesis.

3.3.1 Description of the mesh

To reduce the complexity of the problem the burner was simplified to a two dimensional, axis symmetric mesh with approximately 21 000-25 000 quadratic cells. The mesh can be seen in Figure 18 and Figure 19. In addition, the swirl generator was modeled by defining a tangential velocity as an internal condition where the swirl generator is located. This was done by using an user defined function (UDF) written by Øystein Spangelo [3]. This UDF, written in C-language, multiplies the axial velocity in the cells where it is applied with a tangential angle to create a tangential velocity. The tangential velocity component is defined by equation (3-4), where u_θ is the tangential velocity, u_x is the axial velocity and β is set to 60 degrees. The user defined function can be found in Øystein Spangelo's doctoral thesis.

$$u_\theta = u_x \tan\beta \tag{3-4}$$

The original swirl burner has nozzles both upstream and downstream of the swirl burner. This geometry proved difficult to simulate in FLUENT, due to pressure difference between the gas and burner tube upstream the swirl generator allowing air to seep into the and ignite the fuel inside the gas tube. The problem with the air flowing into the gas tube is visualized in Figure 17. Because of this problem the upstream nozzles in the model were removed, leaving only nozzles downstream of the swirl generator. In order to be able to model the burner as a two dimensional axis symmetric problem, the nozzles were simplified to one hole downstream the swirl generator. The area of the hole is listed as A_{nozzle} in Table 4.

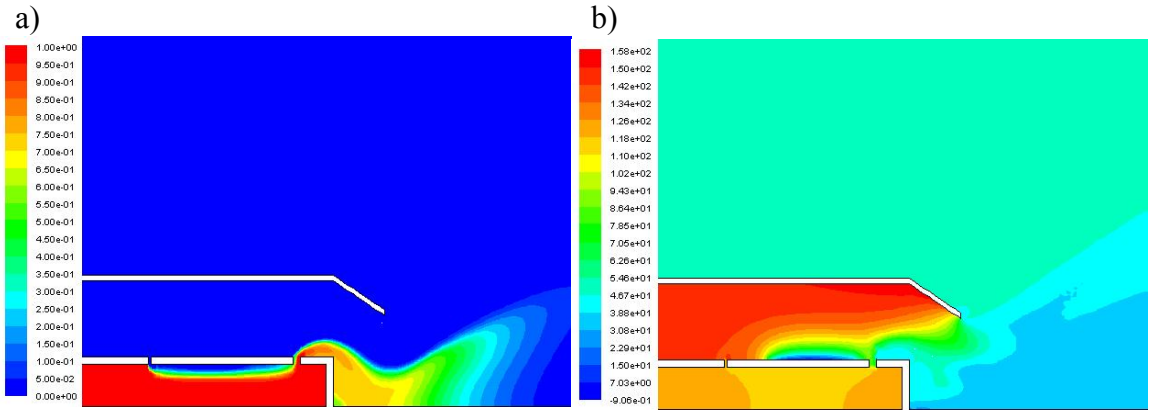

Figure 17: Contours of: a) the mass fraction of C_3H_8 and b) The static pressure in the burner; 10 kW @ 3% O_2 in the flue gas, $\dot{m}_{air}/\dot{m}_{fuel} = 0$ with two nozzle holes

When utilizing these simplifications, the CPU time and memory required to reach convergence are greatly decreased.

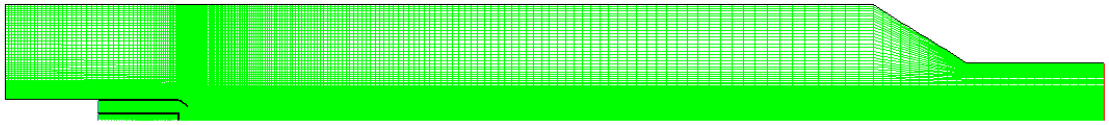

Figure 18: Computational mesh used for the 20 kW swirl burner

The mesh was created in GAMBIT, a mesh preprocessor that interacts with FLUENT. The mesh is structured and created with higher density in areas where the flow is expected to have large gradients, for instance around the fuel nozzles and in the recirculation zones. The number of cells in the mesh depends on the area of the nozzles, because of the increased area with high density cells with increasing nozzle area.

When constructing a mesh it is important to minimize the numerical diffusion (false diffusion). If possible, a structured, quadrilateral mesh with a low skewness should be constructed. A normalized measure of the skewness is defined as follows [6]:

$$Q_{EAS} = \max\left\{\frac{\theta_{\max} - \theta_{eq}}{180 - \theta_{eq}}, \frac{\theta_{eq} - \theta_{\min}}{\theta_{eq}}\right\} \tag{3-5}$$

Where $\theta_{\max}$ and $\theta_{\min}$ are the maximum and minimum angles (in degrees) between the edges of the element, and θ_{eq} is for quadrilateral elements 90˚. By definition, $0 \le Q_{EAS} \le 1$, where $Q_{EAS} = 0$ describes an equilateral element, and $Q_{EAS} = 1$ describes a completely degenerate (poorly shaped) element. For the mesh constructed in this thesis, maximum $Q_{EAS} < 0.39$ and the average $Q_{EAS} << 0{,}1$ which is regarded as an excellent mesh quality [6].

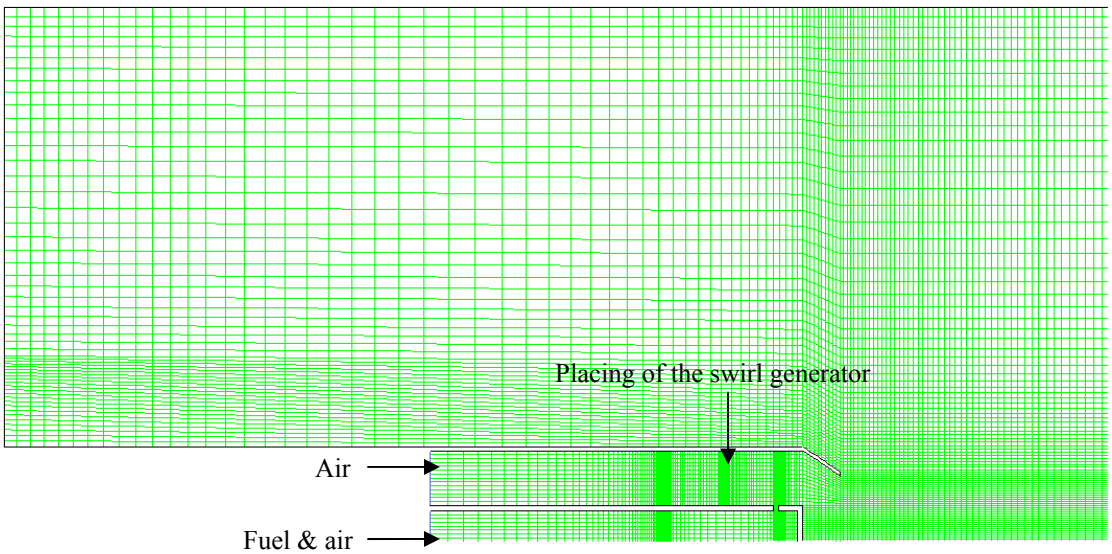

Figure 19: Close-up of the swirl burner with nozzle area calculated for $\dot{m}_{air} / \dot{m}_{fuel} = 0$

3.3.2 Boundary conditions

The calculations were carried out by using the same boundary conditions as in the simulations performed by Øystein Spangelo. These conditions are a model of a water-cooled combustion chamber, and have proven satisfactory in previous calculations [3].

The operating pressure was set to 1.01×10^5 Pascal. The fuel and air flows and different nozzle areas are given for different premixing ratios in Table 4. In Appendix D there is enclosed an excel sheet with dimensions of the swirl burner. The hydraulic diameters for the gas tube, burner tube and the flue gas outlet are respectively 11.5 mm, 20.5 mm and 100 mm. The temperatures were set to 298 K for the incoming fuel and air and 650 K for the flue gas. The bottom of the combustion chamber (left side of Figure 18), the burner tube and the gas tube are all set to insulated steel. On the water-cooled sidewall, the material is steel and the temperature is set to 373 K (boiling water). The conical top and the exhaust pipe is uncooled steel with a constant temperature of 650 K. The temperature is set constant here because of the ambient air's cooling effect. At the outlet the gauge pressure was set to 50 Pascal. When performing experiments in a laboratory there is set a gauge pressure to prevent ambient air to seep into the combustion chamber and change the amount of excess air in the flue outlet. This is of no concern when simulating on the computer, but is included in the model to make it as realistic as possible.

3.3.3 Models used

3.3.3.1 Turbulence and combustion models

From the previous work done on the 20 kW swirl burner, it is concluded that Reynolds stress model (RSM) and flamelet models is the most appropriate respectively turbulence and combustion models [3]. The k-ε turbulence model can on the other hand be used to get more accurate initial conditions before introducing the RSM, and therefore lower the time used on iteration. The constants in the turbulence models are defined by FLUENT, and is not altered.

The flamelet look-up tables were calculated in FLUENT. This proved to be the most time consuming part of the simulations. A look-up table had to be made for each of the different air-fuel ratios because of the composition change in the gas and burner tube. The tables were created as non-adiabatic multiple strained flamelets using the chemical mechanism GRI-Mech 3.0, with 20 different species chosen by FLUENT [26]. A probability density function (PDF) is then calculated from the flamelet table.

3.3.3.2 The solver

The solver used for the computations, was a steady state pressure based implicit two-dimensional swirl solver. The pressure-based solver uses a solution algorithm where the governing equations are solved sequentially (i.e. segregated from one another). Because the governing equations are non-linear and coupled, the solution loop must be carried out iteratively in order to obtain a converged numerical solution, using a second-order scheme. For the pressure interpolation the PRESTO! scheme were used due to recommendation from FLUENT to use this scheme for swirling flows [6]. The difference

between a two dimensional swirl solver and a two dimensional solver is that the circumferential component of velocity is included in the calculations for the swirl solver.

The convergence criteria based on scaled residuals was set to 10^{-4} for all the equations except the energy and radiation equations which was set to 10^{-6}. Before solving the equations, a set of under-relaxation factors can be fixed. The under-relaxation of equations is used in the pressure-based solver to stabilize the convergence behaviour of the outer nonlinear iterations by introducing selective amounts of φ in the system of discretized equations. In a simple form, the new equation value, φ, can be written as follows when implementing the under-relaxation factor α:

$$\varphi = \varphi_{old} + \alpha\Delta\varphi \tag{3-6}$$

These under-relaxation factors proved important when trying to reach the convergence criteria and a lot of effort had to be made to find appropriate values for these factors. An overview of the under-relaxation factors that gave convergence is given in Table 5.

Table 5: Under-relaxation factors used in the simulations

Pressure	Density	Body forces
0.7	0.3	0.7
Momentum	Swirl velocity	Turbulent Kinetic energy
0.3	0.4	0.5
Turbulent dissipation rate	Turbulent viscosity	Reynolds stresses
0.5	0.6	0.5
Pollutant NO	Pollutant hcn	Energy
0.95	0.95	0.99
Temperature	P1	Progress variable
1	0.9	0.9
Mean mixture fraction	Mixture fraction variance	
0.9	0.8	

3.3.3.3 NO_x formation models

The NO_x concentration is in FLUENT calculated in a postprocessor. The postprocessor uses rate models developed at the Department of Fuel and Energy at The University of Leeds in England as well as from the open literature [6]. In the calculations of the NO_x concentrations in this thesis, only models for thermal and prompt NO_x formations are included. In addition a reburn mechanism is implemented, which includes the reduction of NO_x formation by accounting for the reaction of NO with hydrocarbons.

FLUENT solves the mass transport equation for the NO species, taking into account convection, diffusion, production and consumption of NO and related species. This approach is completely general, being derived from the fundamental principle of mass conservation. The effect of residence time in NOx mechanisms, a Lagrangian reference frame concept, is included through the convection terms in the governing equations [6].

The convergence criteria based on scaled residuals was set to 10^{-6} for the transport equation dealing with NO species.

In the calculation of NO from the thermal mechanism, a quasi-steady assumption for the nitrogen concentration is assumed and the NO formation rate can be calculated as follows [6]:

$$\frac{d[NO]_{thermal}}{dt} = 2k_{f,1}[O][N_2]\frac{\left(1-\frac{k_{r,1}k_{r,2}[NO]^2}{k_{f,2}[O_2]+k_{f,3}[OH]}\right)}{\left(1+\frac{k_{r,1}[NO]}{k_{f,2}[O_2]+k_{f,3}[OH]}\right)} \quad \left(\text{gmol/m}^3-s\right) \tag{3-7}$$

Where $k_{i,j}$ is the rate constants for the elementary reactions (2-1), (2-2) and (2-3). The O_2 and OH radical concentration is taken from the local species mass fraction in the flamelet model.

The prompt NO_x formation rate is calculated from equation (3-8) [6]:

$$\frac{d[NO]_{prompt}}{dt} = fk_{pr}[O_2]^a[N_2][FUEL]e^{-E_a/RT} \tag{3-8}$$

Where f is a correction factor that incorporates the effect of the fuel type and equivalence ratio, k_{pr} is the rate coefficient, a is the oxygen reaction order, E_a is the activation energy, R is the universal gas constant and T is the temperature.

3.3.4 Comparison of the calculations with previous work

As mentioned previously, there has been performed some work with the swirl burner in the past both experimental in the laboratory and CFD simulations in FLUENT. The results from the previous work can be used to validate accurateness of the CDF calculations. In this chapter the results from the calculations of the swirl burner at 10 kW with $\dot{m}_{air}/\dot{m}_{fuel} = 0 \Rightarrow \phi_{local} = \infty$ performed here will be compared with previous measurements and calculations made on the same burner.

In a strong swirling flow it is important to be able to model the central toroidal recirculation zone (CTRZ) and the corner recirculation zone (CRZ). Figure 20 indicates the contours of the zero-axial velocity areas in the combustion chamber from the new calculations performed here and the old ones performed by Øystein Spangelo. In Figure 20 it can be seen that the new calculations manage to model the recirculation zones described in chapter 2.2.3. When comparing the new calculations with the old one, the recirculation zones seem more stretched out in axial direction and not as plump as in Spangelo's calculations. The reason for these differences is not found, but since the same models and solvers are employed in the two calculations the source of the differences has

to be the flamelet look-up tables, the mesh, the nozzle geometry or the placing of the swirl generator.

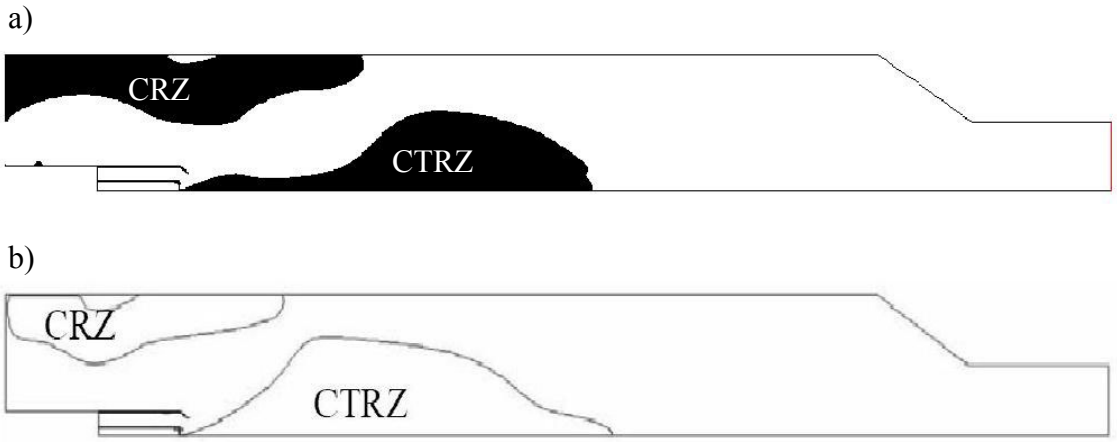

Figure 20: Contours of zero-axial velocities: a)The new calculations in this thesis; b) Calculations by Øystein Spangelo, 10 kW @ 3% O_2 with $\dot{m}_{air}/\dot{m}_{fuel} = 0$ [3]

As described in chapter 2.1, temperature is an important parameter considering NO_x emissions. A verification of the correctness of the calculated temperature should therefore be made. At the moment there exists no successful experimental measurement of the temperature distribution in the swirl burner. Spangelo investigated the possibility to use laser induced fluorescence (LIF) for temperature measurements, but the LIF was found too inaccurate [3]. One property that it is possible to compare the calculated temperature with is the adiabatic flame temperature for propane listed in Table 1 in chapter 2.3. The maximum calculated temperature should be below the adiabatic flame temperature because of for instance heat loss, recirculation zones, excess air in the flue gas or dissociation of the combustion products [20]. The adiabatic flame temperature for propane is 1994 ˚C. The maximum temperature calculated in FLUENT with the help of the models described in the previous chapter was 1706 ˚C (see Figure 29 in Appendix B). Spangelo calculated a maximum temperature of 1700 ˚C. A temperature around 1700-1706 ˚C can therefore be a feasible temperature for the burner, but without experimental values no final conclusion can made about its correctness.

Another parameter that affects the NO_x emissions is the shape of the flame. The size of the high temperature area will effect the emissions significantly. One way of to describe the flame shape is to look at the OH concentration in the combustion chamber. Formation of OH radicals takes place in the flame front and is in most flames present in relatively large concentrations. The OH radical is therefore, together with CH radical, a typical marker of the flame front [3]. Figure 21 and Figure 22 shows the results of Spangelo's work with LIF measurements and calculations in FLUENT, respectively. Spangelo had some problems to reproduce the flame shape that was measured with the LIF. The range of the OH concentrations is satisfactory, but the flame shape in the calculation looks more like a "flower" and is far more divergent than the measured shape. This "flower" shape can also be seen from the new calculations performed in this thesis (see Figure 23), except that it is more closed and not that divergent as the flame in Spangelo's

calculations. It seems like the new calculations can model the flame shape better than the old one performed by Spangelo.

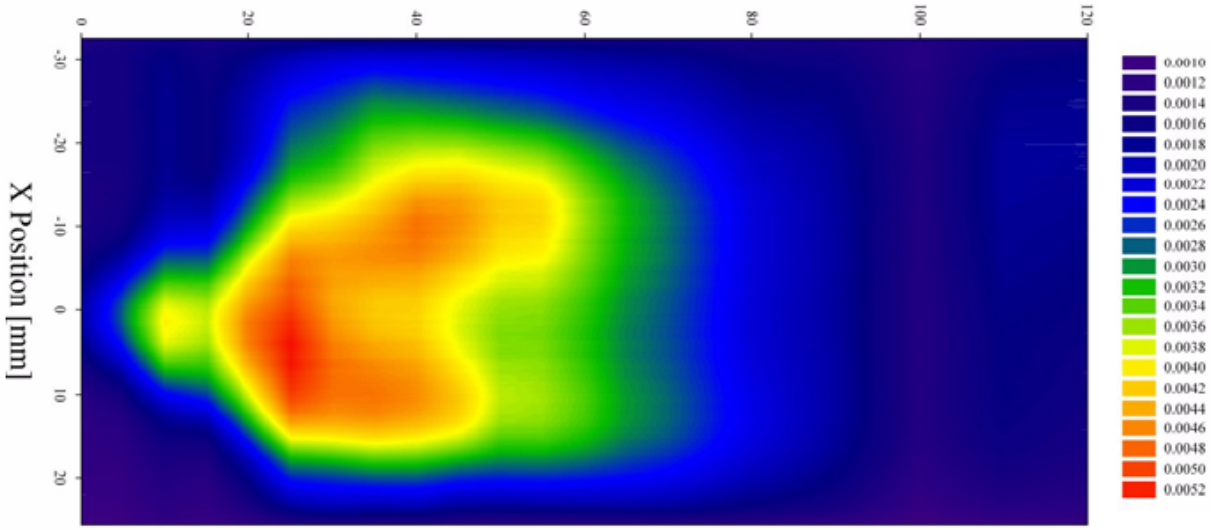

Figure 21: OH mole fractions in swirl burner measured with LIF, 10 kW @ 3% O_2 [3]

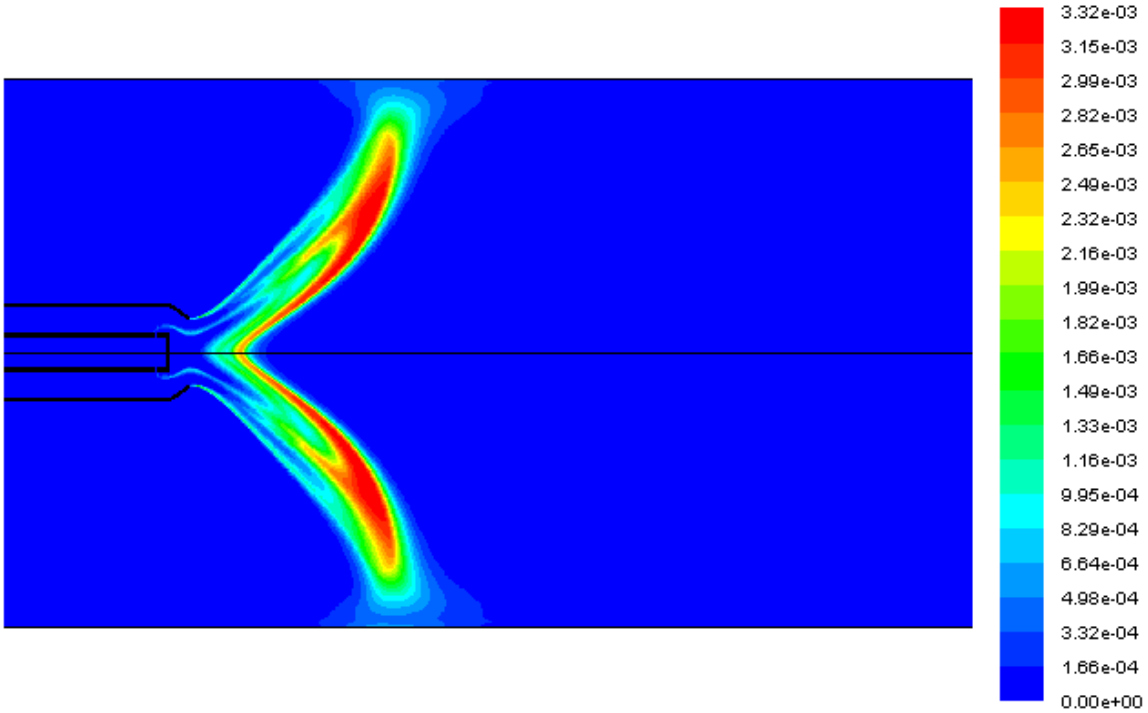

Figure 22: OH mole fractions computed in FLUENT by Øystein Spangelo, 10 kW @ 3% O_2 [3]

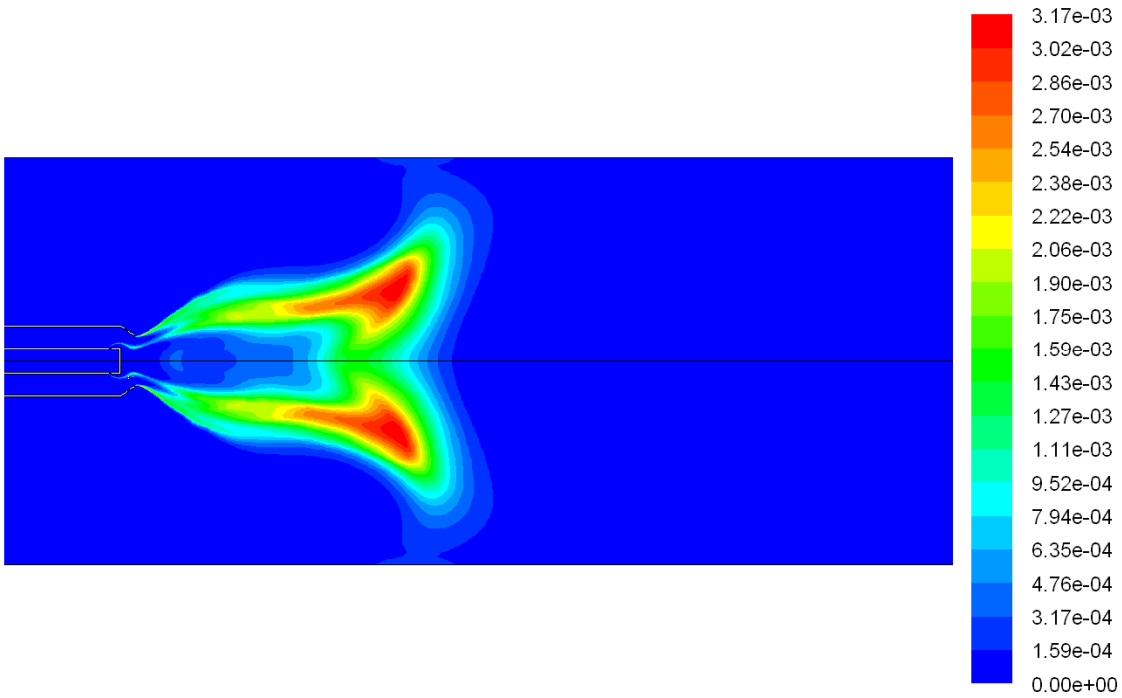

Figure 23: OH mole fractions computed in FLUENT, $\dot{m}_{air}/\dot{m}_{fuel} = 0$ 10 kW @ 3% O_2

The problem described in chapter 3.3.1 with air seeping into and igniting in the gas tube was not a problem when removing the nozzle upstream of the swirl generator. The contours of the C_3H_8 mass fraction and the static pressure is given in Figure 24.

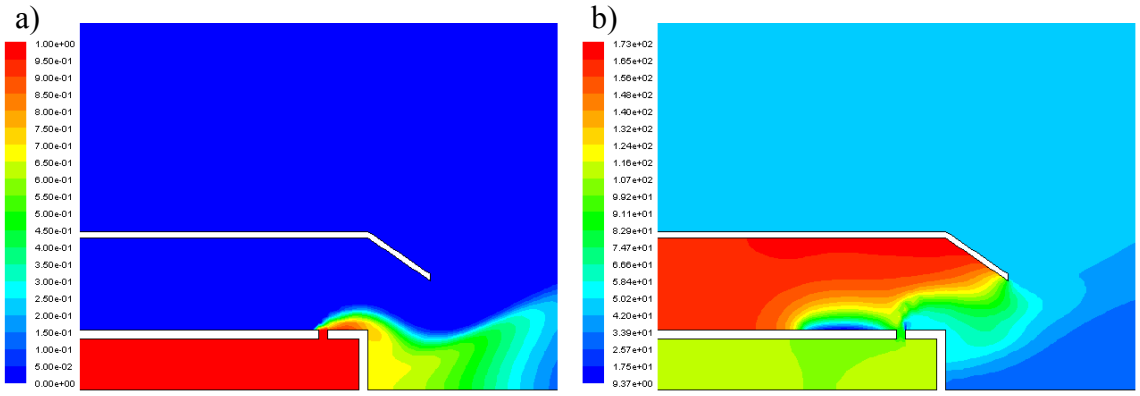

Figure 24: Contours of: a) the mass fraction of C_3H_8 and b) The static pressure in the burner; 10 kW @ 3% O_2, $\dot{m}_{air}/\dot{m}_{fuel} = 0$ with one nozzle hole

3.4 The effect of partial premixing on NO_x emissions

In Figure 25 the NO_x concentration from the simulations of the 10 kW swirl burner is plotted versus the different premixing ratios listed in Table 4. The quantity of the NO_x emission is different from the results found from experimental measurements. Spangelo measured a NO_x concentration of approximately 26 ppmv when performing experiments with the swirl burner at 10 kW power output, three percent excess air and no premixing [3]. In the simulations, an emission of 0.5 ppmv was calculated. This difference was, as explained earlier, expected. The interesting thing is to see what effect partial premixing have on the NO_x emission. This will be expounded in the following sections.

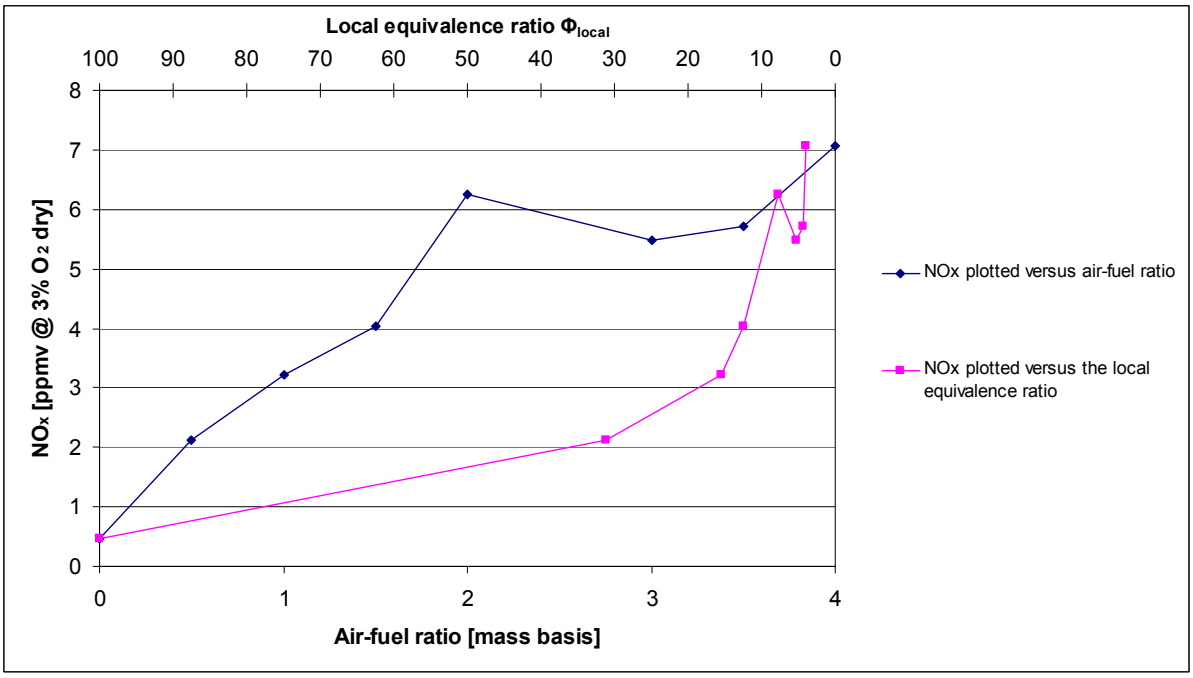

Figure 25: Simulated concentration of NO_x in the flue gas plotted versus the air-fuel ratio and the local equivalence ratio in the gas tube

The NO_x concentration increases when going from a diffusion flame to a partially premixed flame, and reaches a temporary peak at an air-fuel ratio of two ($\phi_{local} \approx 7.8$). When the air-fuel ratio exceeds two, the NO_x concentration decreases until it reach an air-fuel ratio of three ($\phi_{local} \approx 5.2$). This is in good accordance with the experiments performed by Turns et al. plotted in Figure 14 on page 15. When further increasing the air-fuel ratio towards the upper flammability limit the NO_x concentration starts to increase again. This local minimum in the range $2 < \dot{m}_{air} / \dot{m}_{fuel} < 3.5$ $(7.8 < \phi_{local} < 4.4)$ when premixing air and propane, is the same phenomena that is observed using methane as fuel (see chapter 2.2.2: Partially premixed flames). The difference between the two fuels is that when premixing air and methane it exist a global minimum in the NO_x emissions, while for propane the global minimum in NO_x emissions is for zero premixing, i.e. diffusion flame. The conclusion is therefore that premixing air and propane will not give a reduction in the NO_x emissions when comparing with a diffusive propane flame.

In Figure 26, the maximum flame temperature in the combustion chamber is plotted versus the air-fuel ratio. The temperature rises quite steep when going from diffusion flame to an air-fuel ratio of two and then stabilizing at a temperature around 1915-1955 ˚C. The variation in NO_x concentration between the different air-fuel ratios can therefore not be explained by the maximum temperature in the combustion chamber alone, but it is clear that the thermal NO_x formation mechanism is an important parameter.

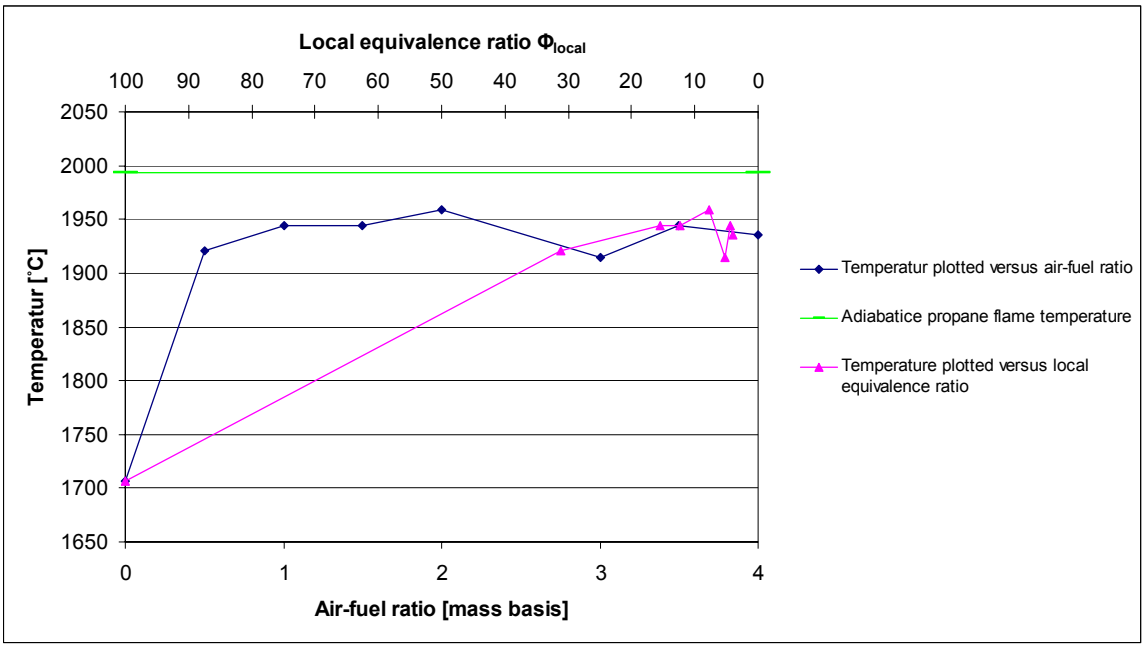

Figure 26: Simulated maximum flame temperature in the combustion chamber [˚C]

In Appendix B contours of temperature, OH mole fraction and zero-axial velocities for different air-fuel ratios are visualized. A comparison of the different contours between the air-fuel ratios of 0.5 and 4 are given in Figure 27. These two ratios have a difference in the NO_x concentration in the flue gas of approximately 5 ppmv even though the difference in maximum flame temperature is only 16 ˚C. The reason for this difference is mainly due to a larger high temperature flame region for the air-fuel ratio of 4 which will benefit thermal NO_x formation. This can also be seen from the increased OH concentration area in Appendix B. Another interesting observation is the decreasing central toroidal recirculation zone for increasing air-fuel ratios. A reduction in the recirculation zone will raise the temperature and the O_2 partial pressure in the flame. The result from the simulations implies that the NO_x reduction due to swirl generation is almost none existing for higher air-fuel ratios.

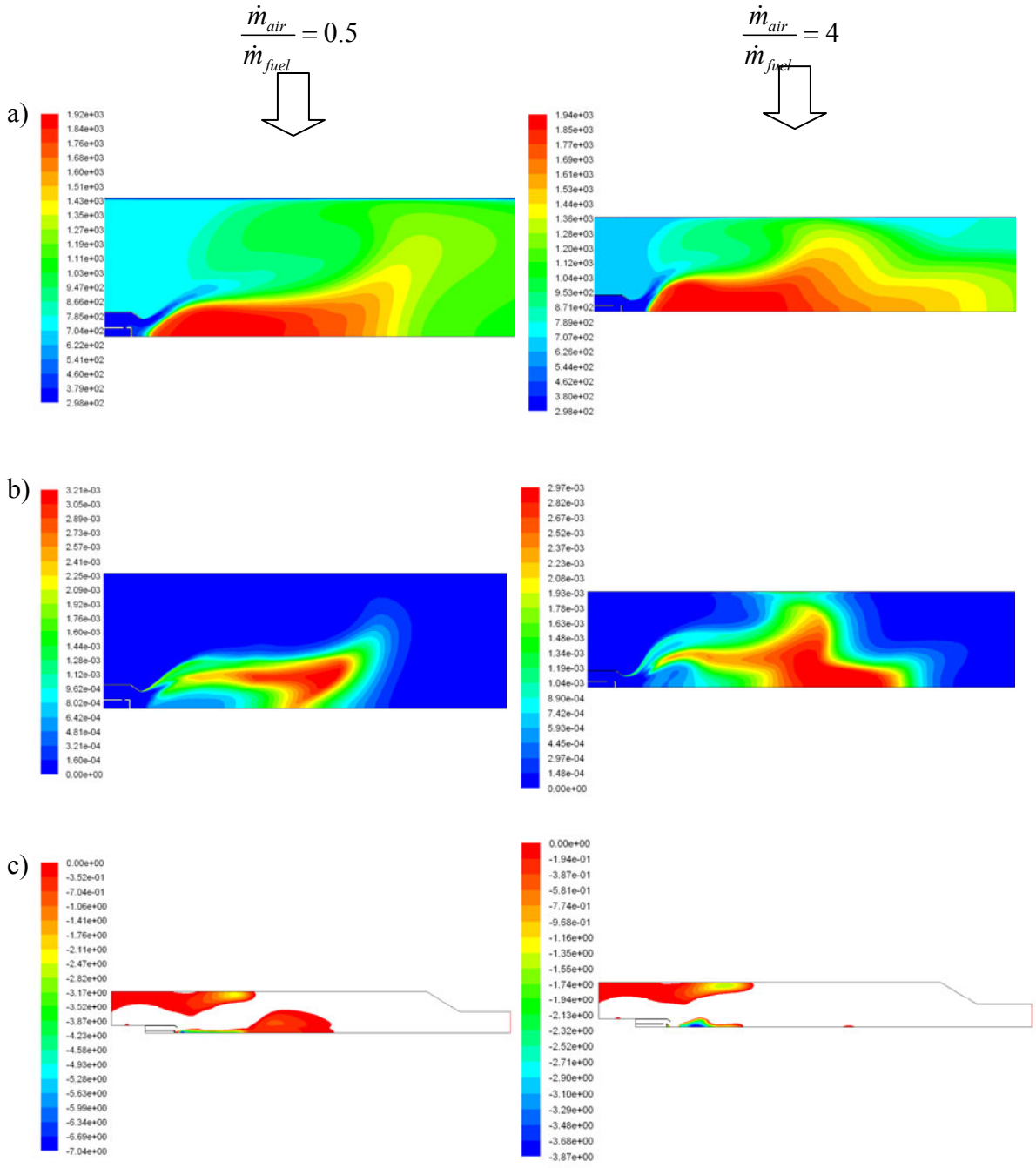

Figure 27: Comparison of: a) Temperature contours; b) OH mole fraction; c) recirculation zones for the air-fuel ratios of 0.5 and 4

From equation (2-6) and (2-7) in chapter 2.1, it can be seen that HCN is an intermediate product in the prompt NO_x formation mechanism. So to investigate if it is an increase in the prompt NO_x formation that causes the differences in NO_x concentration, the HCN mole fractions at different air-fuel ratios were compared in Figure 53 on page 57. The figure tells us that the maximum HCN concentration in the combustion chamber decreases with increasing air-fuel ratios, and that the size of the HCN formation area remains relatively constant. The prompt NO_x formation will therefore decrease with increasing air-fuel ratios.

4 Conclusion and recommendations for further work

4.1 Conclusion

Combustion simulations have bee performed on a 20 kW swirl burner with the use of the commercial CFD software FLUENT. The effect of premixing air and fuel on NO_x emissions was investigated. Due to previous experimental problems with stability in the actual burner when burning methane, propane was chosen as fuel.

In the literature study, premixing air and methane were found to decrease the NO_x emissions for a specific range of higher air-fuel ratios. For propane no complete analyses of this topic were found, however some experiments with lower air-fuel ratios indicates an increase in the NO_x emissions.

For modeling of the 20kW swirl burner, a 2D structured grid consisting of about 21 000-25 000 cells were created in GAMBIT. The grid was imported into FLUENT where simulations of eight different premixed air-fuel ratios at a thermal throughput of 10 kW were performed. For the modeling of turbulence the Reynolds Stress Model was employed, while the PDF Flamelet model was used for modeling combustion. The results from the simulations proved satisfactory when comparing with previous work done on the same burner. The exception was the NO_x emission, which could not be calculated exactly. This is a common known problem in FLUENT and CFD software in general, and correct physical quantities of NO_x concentration were not expected to be found.

The conclusion regarding the effect of partial premixing on NO_x emissions is that when using propane as fuel, there is no positive effect on the NO_x emissions. Some of the same trends can be seen when increasing the premixing air-fuel ratio for propane and methane, but for propane the overall NO_x concentration is higher than for a diffusion flame. This implies that reduction of NO_x emissions by partial premixing is strongly fuel dependent. The reason for this increase in NO_x is found to be mainly because of a growing high temperature flame zone and a reduction in the central toroidal recirculation zone for higher air-fuel ratios. The formation of NO_x through the prompt mechanism is found to slightly decrease when the air-fuel ratio is increased, and this mechanism is therefore not contributing to the raise in the NO_x concentrations.

4.2 Recommendations for further work

Experimental measurements of temperature and NO_x concentrations at different premixing ratios should be carried out. Results from experiments could help verifying the results from the simulations of the swirl burner. If the simulations appear to be inaccurate, measures to improve the model should be made. These measures could for instance be to improve the boundary conditions (to import velocity, temperature profiles etc.), to model the swirl burner in 3D or to change turbulence and reaction models. Also, a LIF measurement of the temperature could help investigate if the increase in the NO_x emissions when partial premixing is implemented is because of a larger high temperature area in the combustion chamber.

A larger number of simulations or experiments at different air-fuel ratios should also be carried out, especially around ratios between 2 and 3.5. More simulations could give answer to if the local minimum in this range is lower than the one found in this thesis.

If an up scaled version of the swirl burner is used, there is possible to apply both propane and methane as fuel. This will give an interesting comparison of the differences between the fuels, which was not possible when using the 20 kW swirl burner.

Appendix A Calculations

A.1 Calculations of new nozzle area with varying partial premixing

Based on pressure measurements, the fuel injected into the oxidizer is found to be distributed with 35% upstream and 65% downstream of the swirl generator [3]. This distribution proved difficult to simulate in FLUENT and problems with air seeping into the gas tube occurred (See Figure 17 in chapter 3.3.1). The nozzle upstream of the swirl generator was therefore removed and only the downstream nozzle is included in the constant velocity calculations.

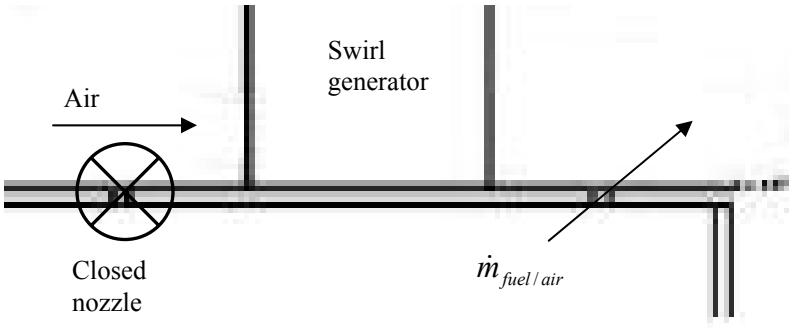

Figure 28: Illustration of fuel distribution in the burner

The original nozzle velocity was calculated with the following equation:

$$v_{nozzle} = \frac{\dot{m}_{fuel}}{\rho_{fuel} A_{nozzle}} \tag{4-1}$$

v_{nozzle}	Velocity in nozzle upstream the swirl generator
$\dot{m}_{fuel}$	Fuel pipe mass flow
ρ_{fuel}	density of the fuel
A_{nozzle}	Area of the nozzles

By setting the velocity in the nozzle constant and then rearranging equation (4-1), the new nozzle area with a different fuel-air mass flow can be found:

$$A_{nozzle}^{new} = \frac{\dot{m}_{mix}}{\rho_{mix} v_{nozzle}} \tag{4-2}$$

Where ρ_{mix} can be found by applying equation (4-3):

$$\rho_{mix} = \frac{1}{\left(mf_{fuel} \frac{1}{\rho_{fuel}} + mf_{air} \frac{1}{\rho_{air}} \right)} \tag{4-3}$$

Where mf_i is the mass fraction of fuel and air.

Appendix B Some results from the simulations

B.1 Contours with premixed air-fuel ratio equal to 0

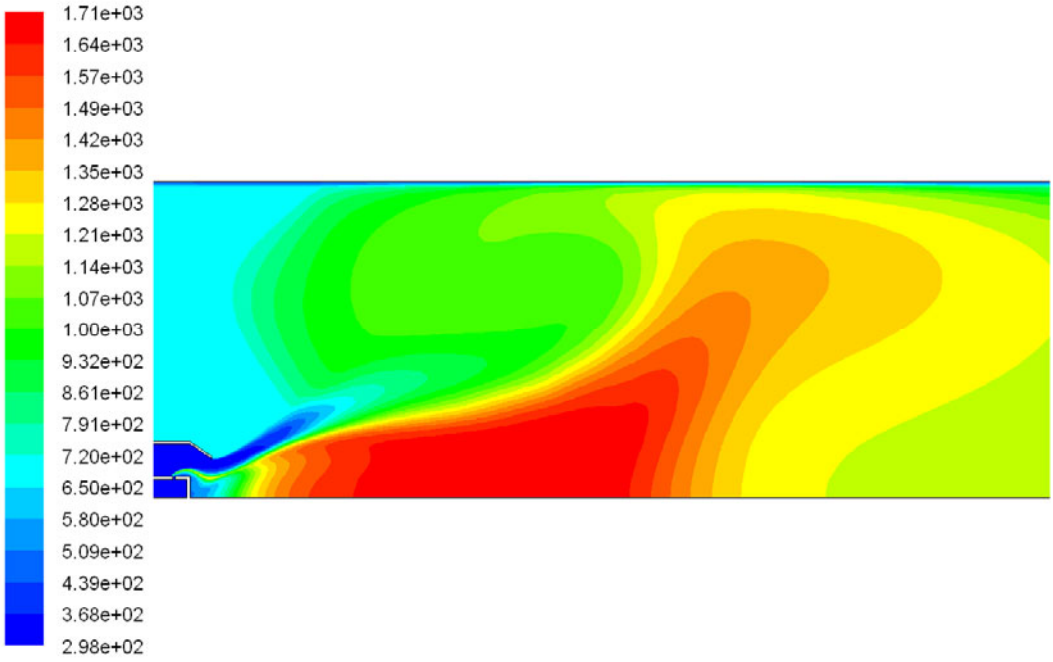

Figure 29: Contours of temperature [˚C], 10 kW @ 3% O_2 with $\dot{m}_{air} / \dot{m}_{fuel} = 0$

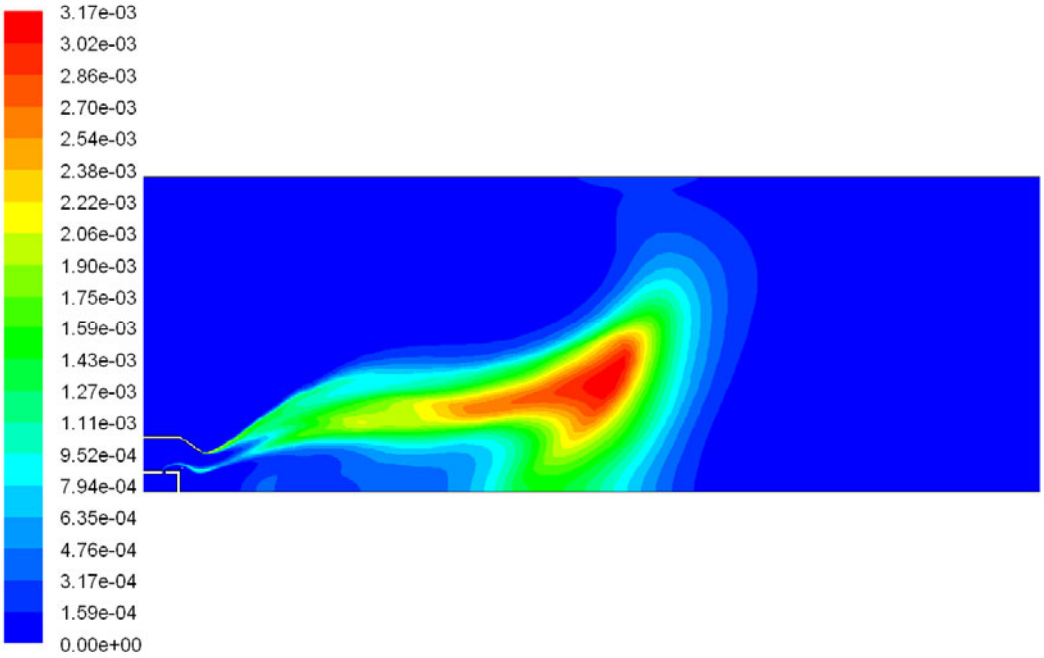

Figure 30: Contours of OH mole fraction, 10 kW @ 3% O_2 with $\dot{m}_{air} / \dot{m}_{fuel} = 0$

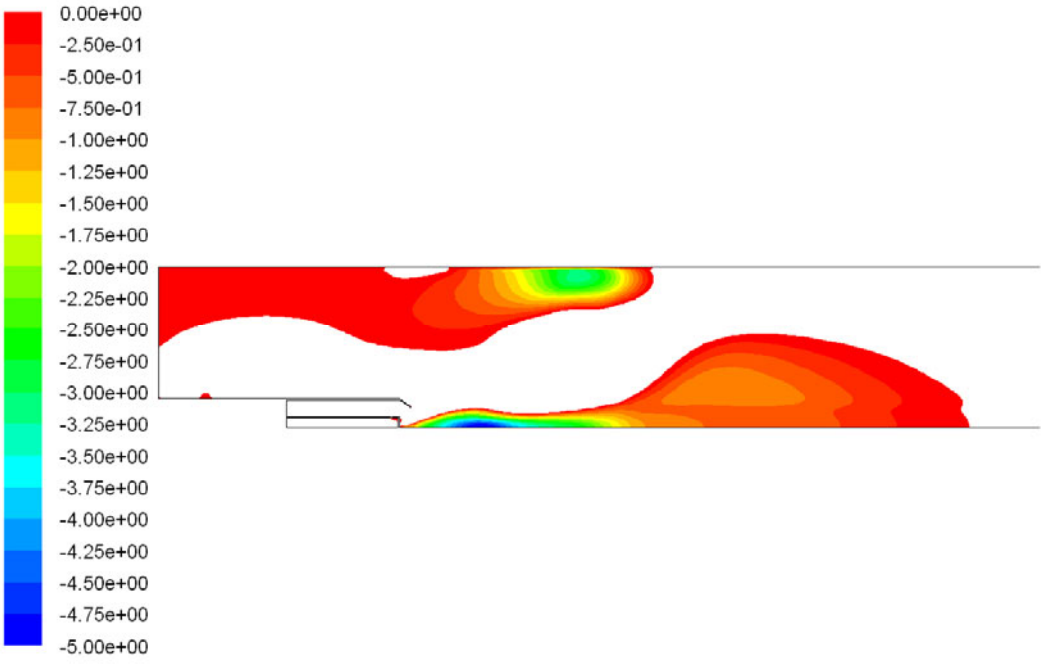

Figure 31: Contours of zero-axial velocities [m/s], 10 kW @ 3% O_2 with $\dot{m}_{air}/\dot{m}_{fuel} = 0$

B.2 Contours with premixed air-fuel ratio equal to 0.5

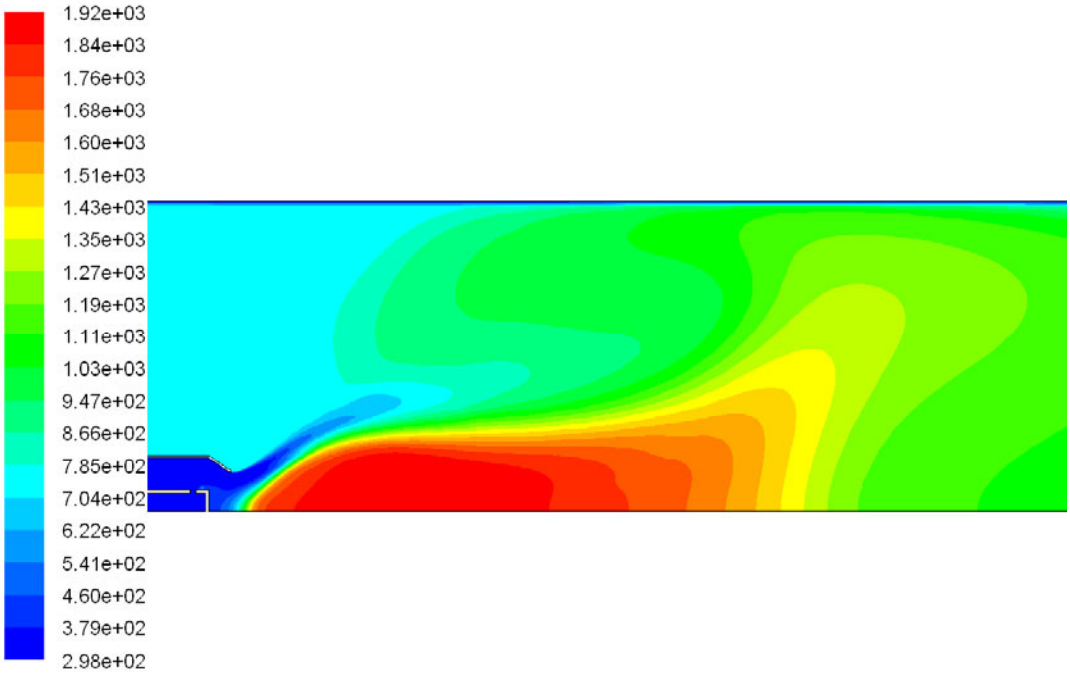

Figure 32: Contours of temperature [˚C], 10 kW @ 3% O_2 with $\dot{m}_{air}/\dot{m}_{fuel} = 0.5$

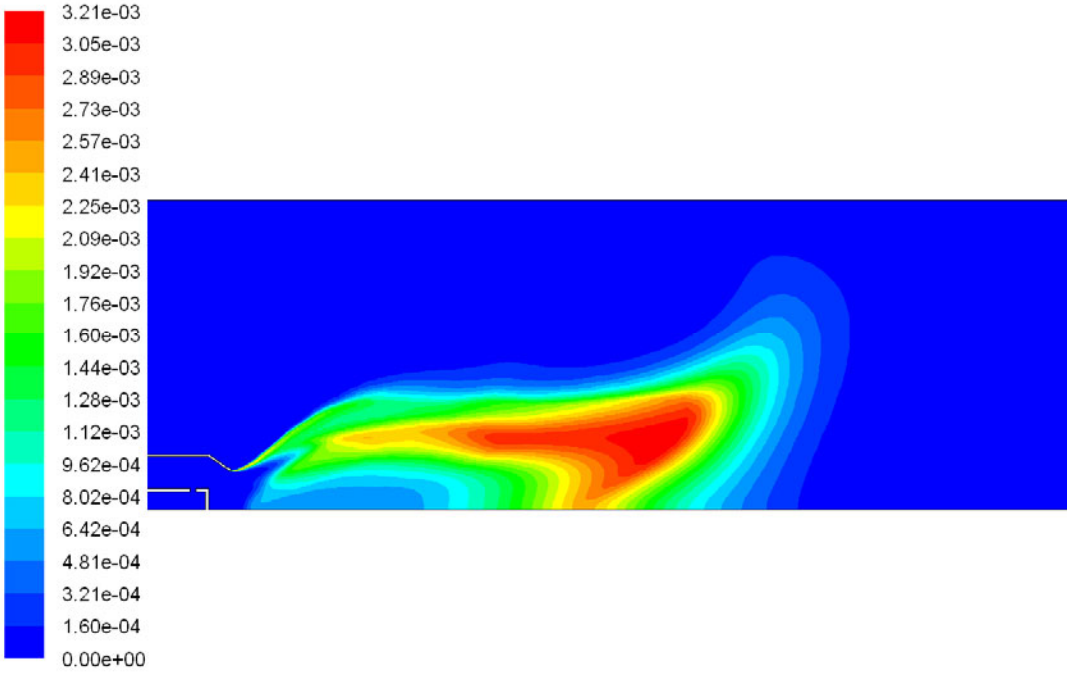

Figure 33: Contours of OH mole fraction, 10 kW @ 3% O_2 with $\dot{m}_{air}/\dot{m}_{fuel} = 0.5$

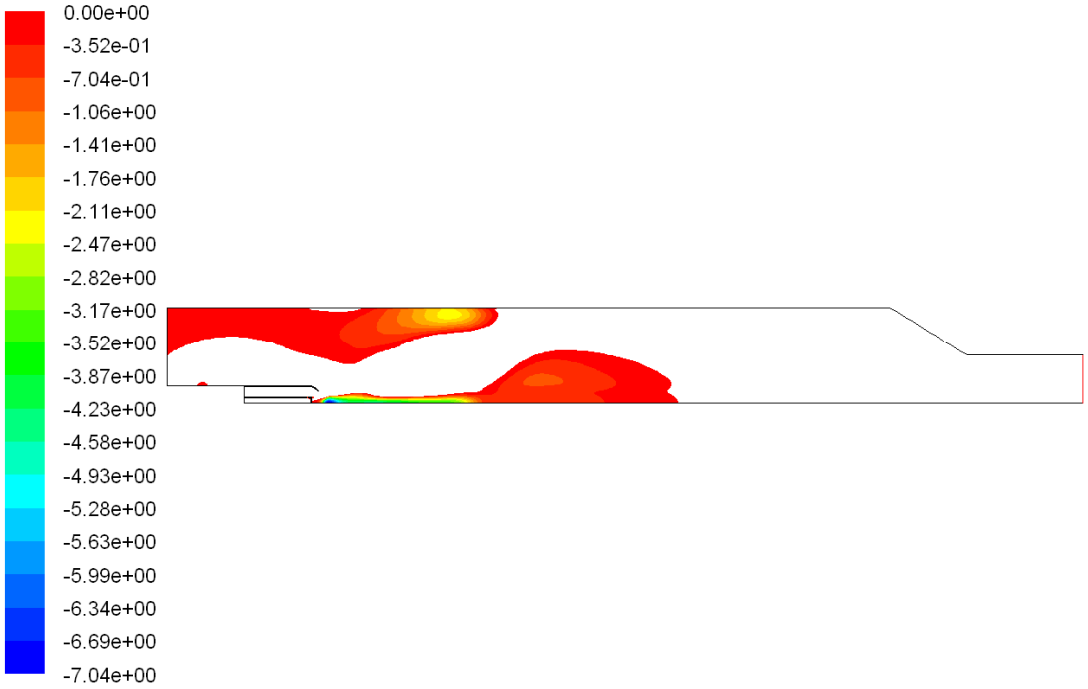

Figure 34: Contours of zero-axial velocities [m/s], 10 kW @ 3% O_2 with $\dot{m}_{air}/\dot{m}_{fuel} = 0.5$

B.3 Contours with premixed air-fuel ratio equal to 1

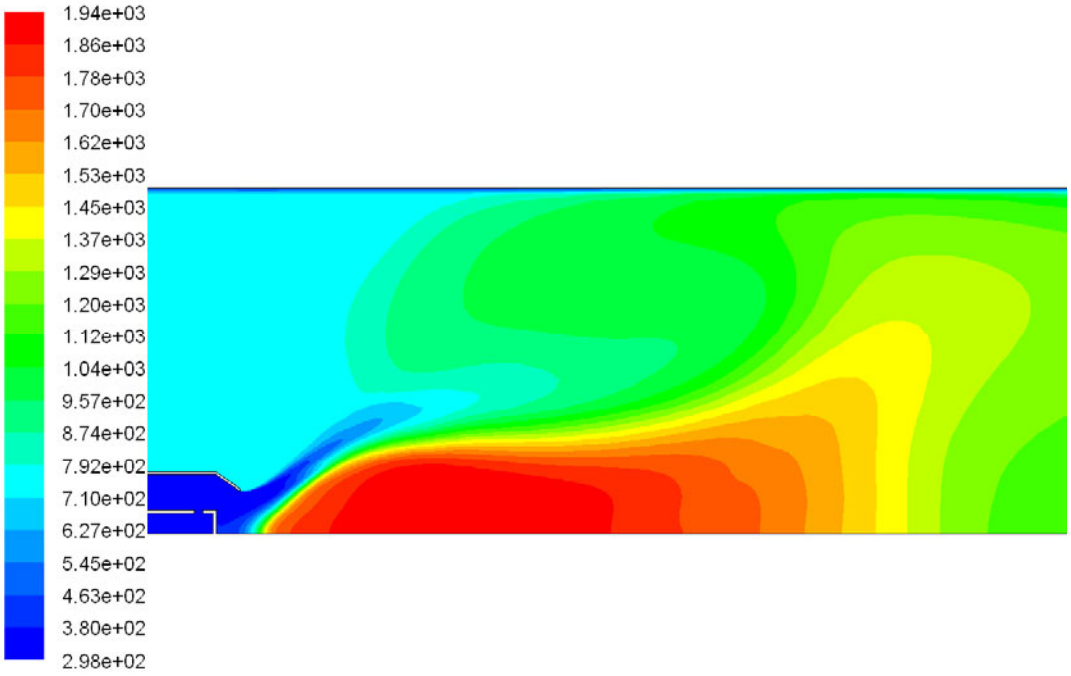

Figure 35: Contours of temperature [˚C], 10 kW @ 3% O_2 with $\dot{m}_{air} / \dot{m}_{fuel} = 1$

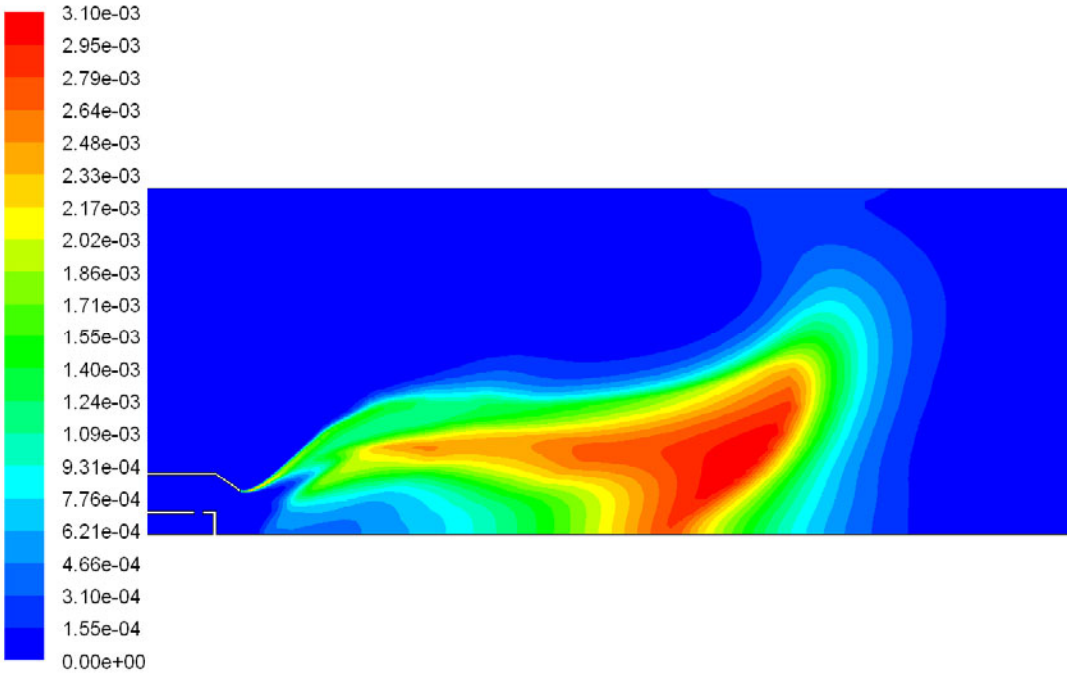

Figure 36: Contours of OH mole fraction, 10 kW @ 3% O_2 with $\dot{m}_{air} / \dot{m}_{fuel} = 1$

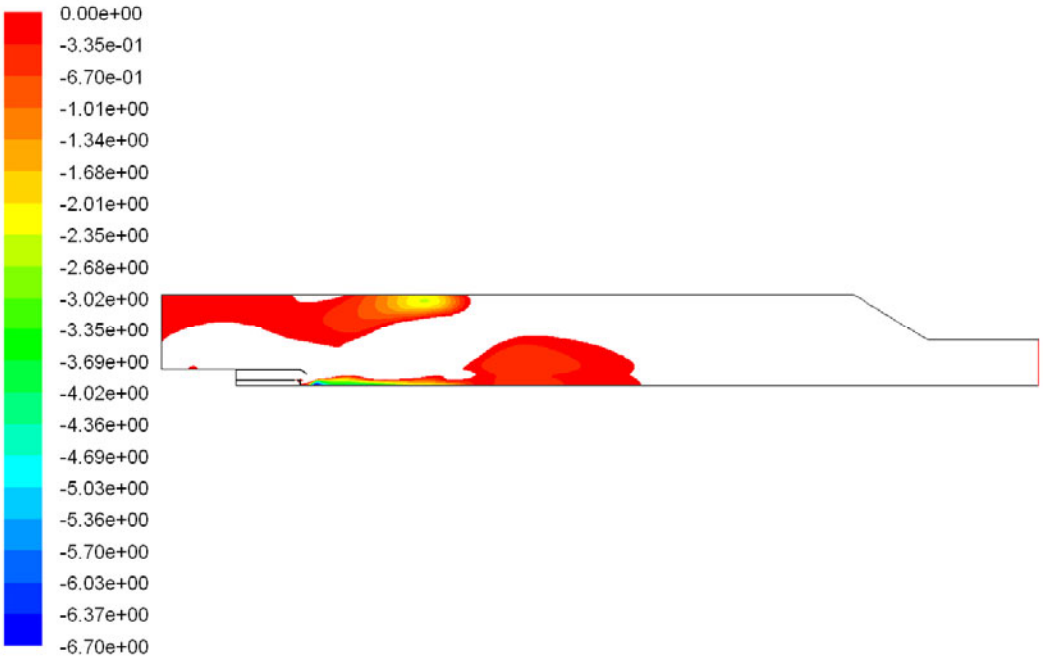

Figure 37: Contours of zero-axial velocities [m/s], 10 kW @ 3% O_2 with $\dot{m}_{air} / \dot{m}_{fuel} = 1$

B.4 Contours with premixed air-fuel ratio equal to 1.5

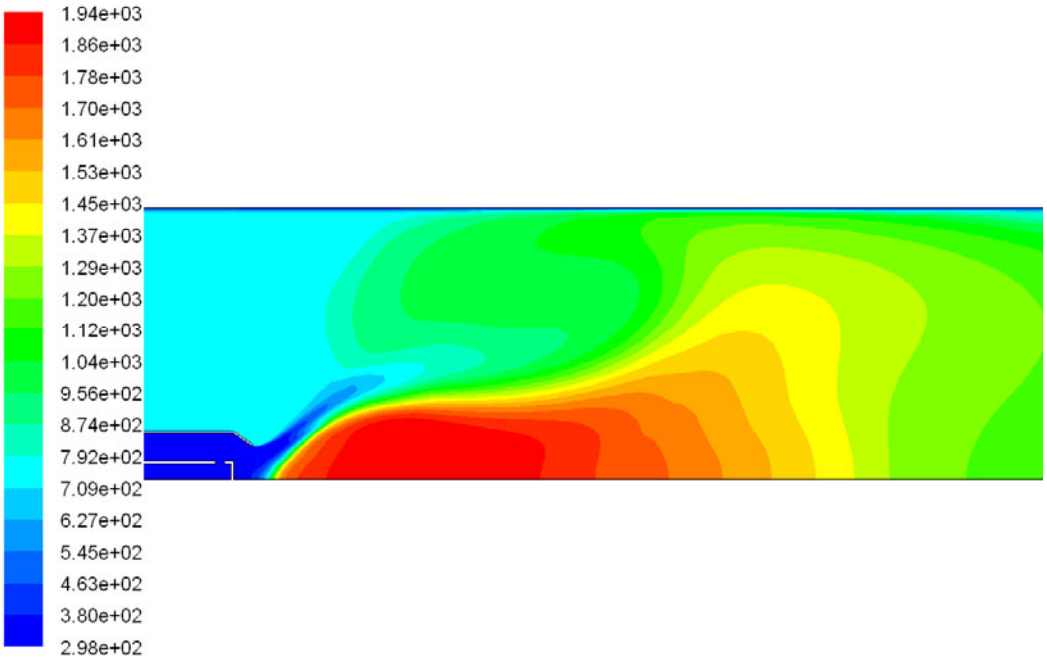

Figure 38: Contours of temperature [˚C], 10 kW @ 3% O_2 with $\dot{m}_{air} / \dot{m}_{fuel} = 1.5$

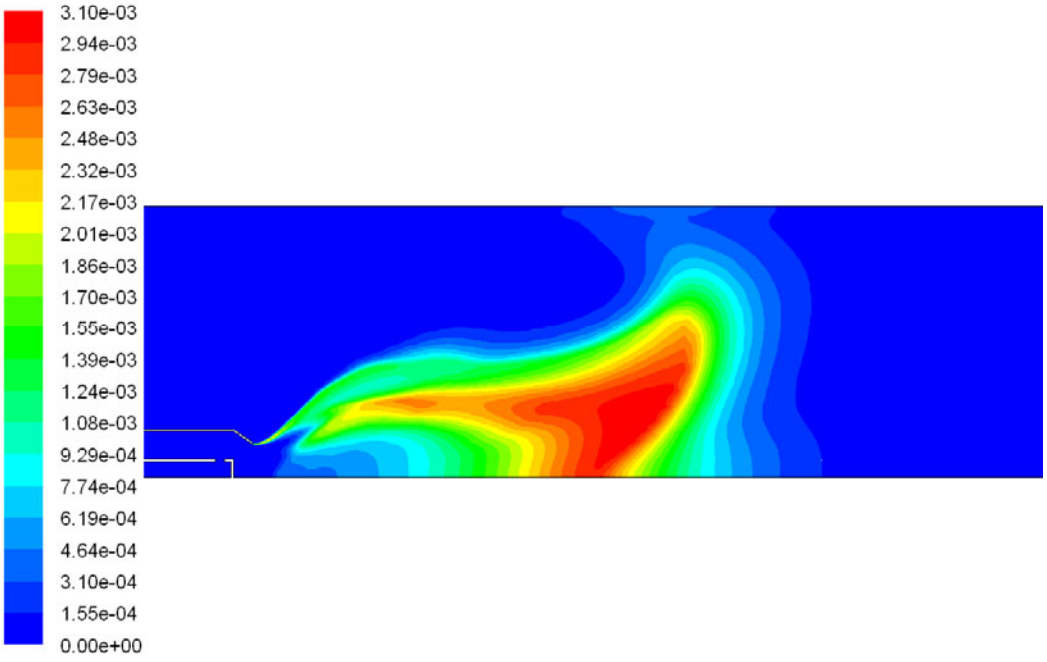

Figure 39: Contours of OH mole fraction, 10 kW @ 3% O_2 with $\dot{m}_{air}/\dot{m}_{fuel} = 1.5$

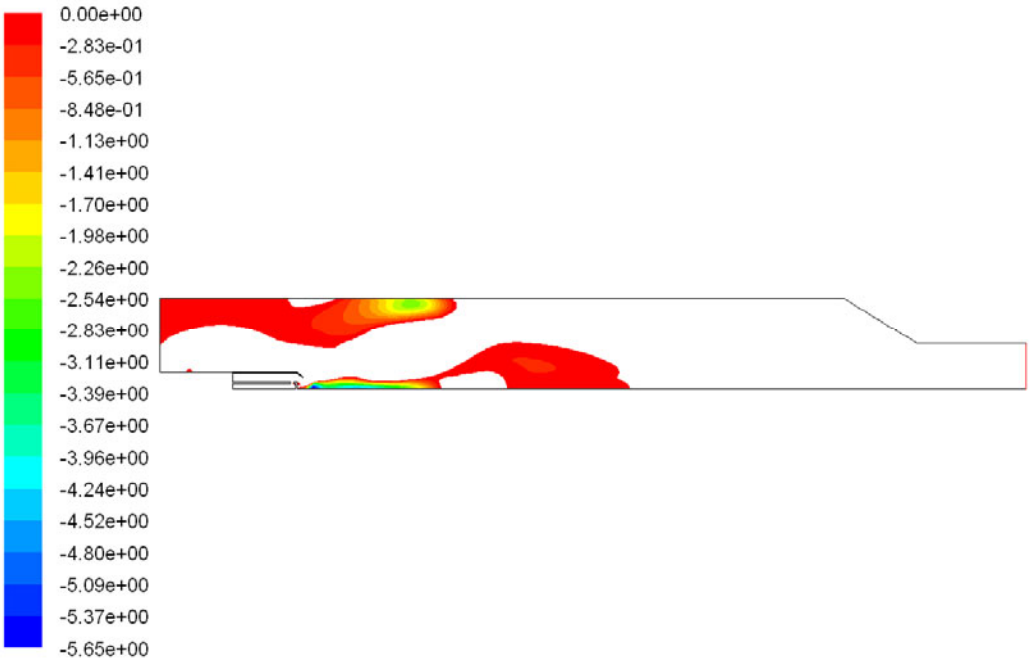

Figure 40: Contours of zero-axial velocities [m/s], 10 kW @ 3% O_2 with $\dot{m}_{air}/\dot{m}_{fuel} = 1.5$

B.5 Contours with premixed air-fuel ratio equal to 2

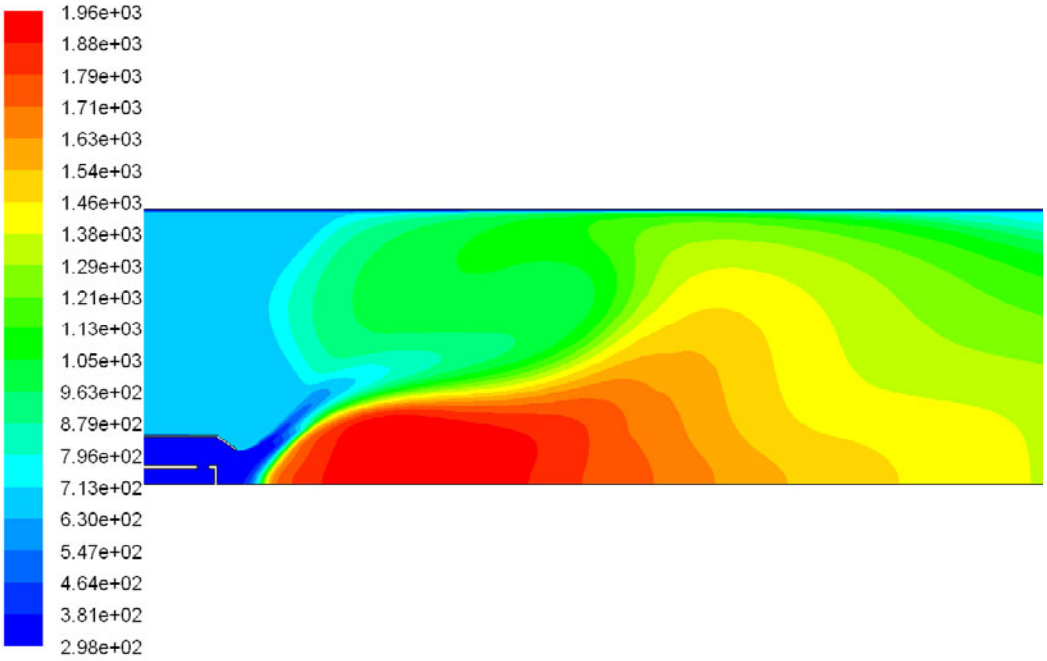

Figure 41: Contours of temperature [˚C], 10 kW @ 3% O_2 with $\dot{m}_{air} / \dot{m}_{fuel} = 2$

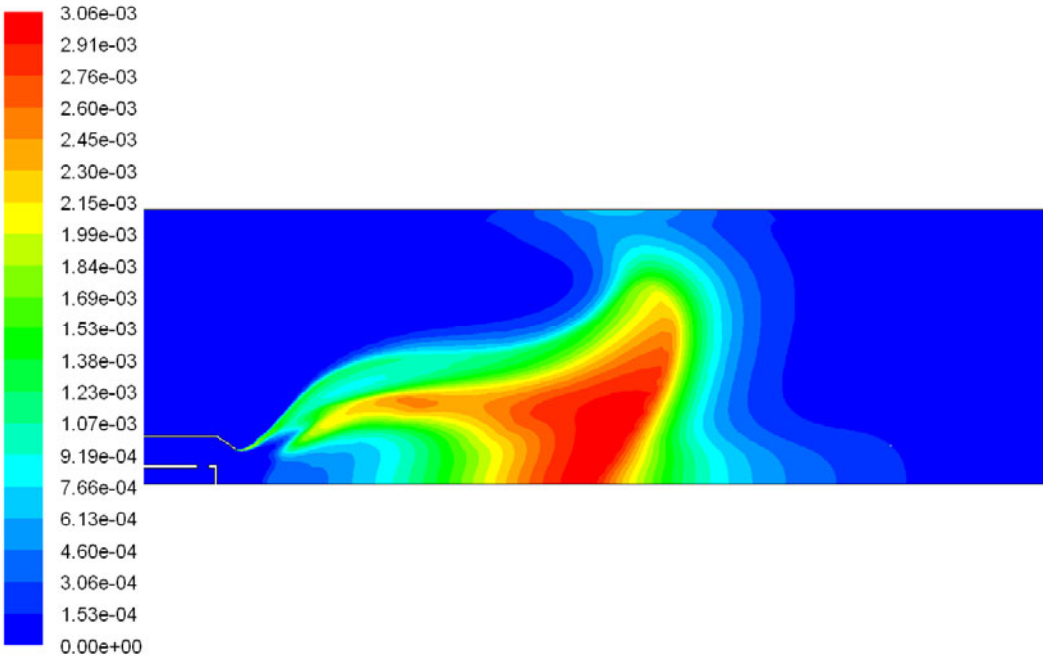

Figure 42: Contours of OH mole fraction, 10 kW @ 3% O_2 with $\dot{m}_{air} / \dot{m}_{fuel} = 2$

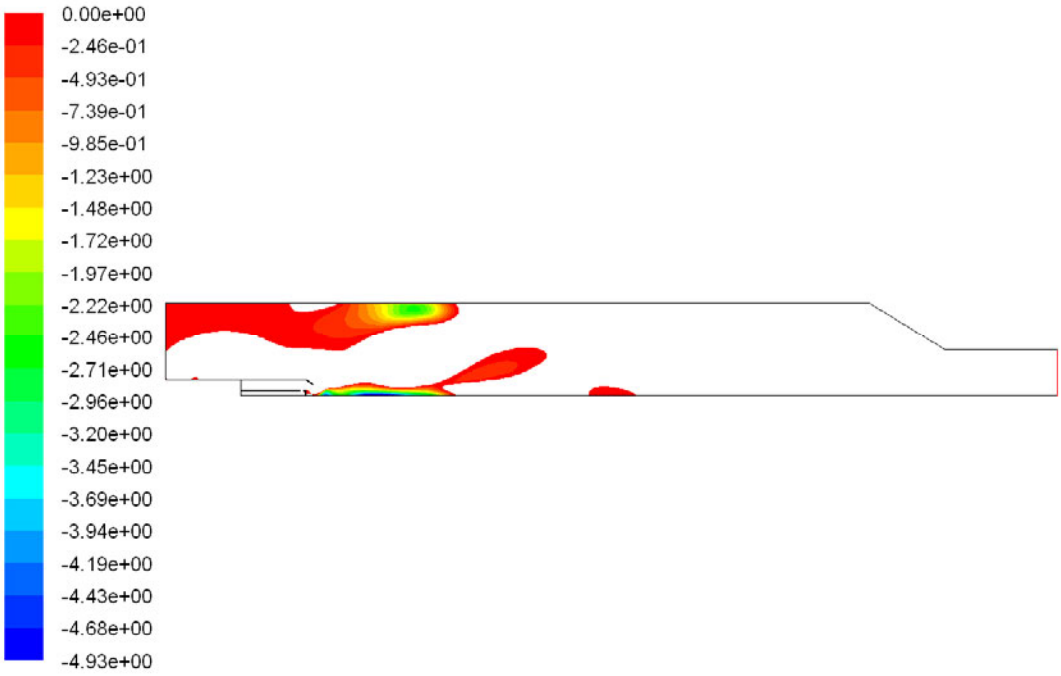

Figure 43: Contours of zero-axial velocities [m/s], 10 kW @ 3% O_2 with $\dot{m}_{air} / \dot{m}_{fuel} = 2$

B.6 Contours with premixed air-fuel ratio equal to 3

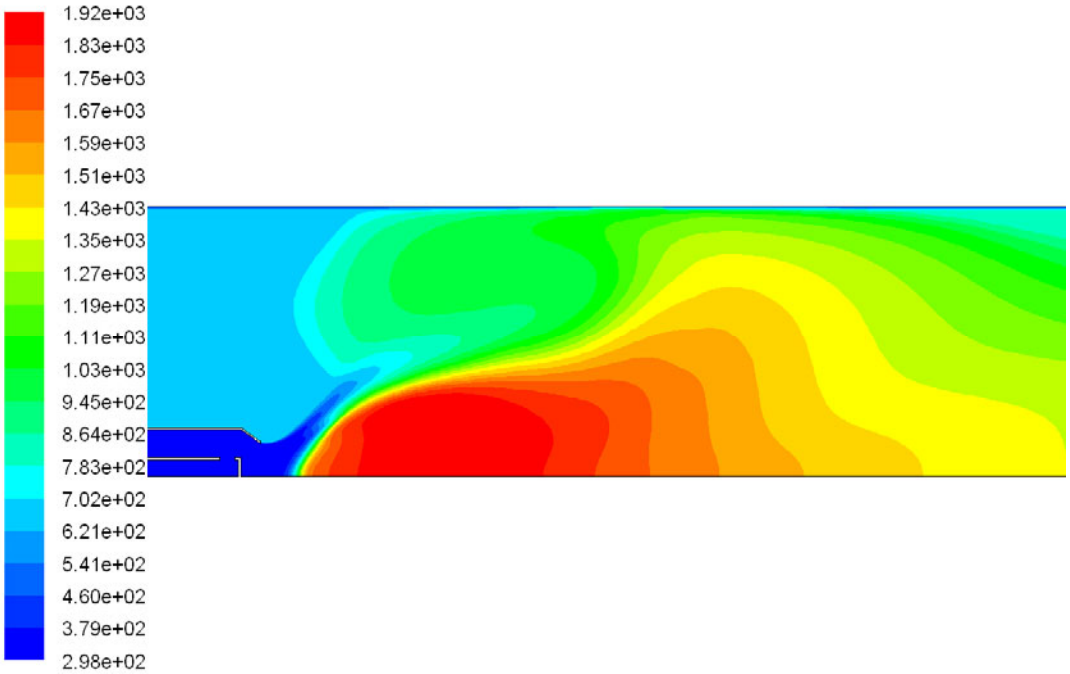

Figure 44: Contours of temperature [˚C], 10 kW @ 3% O_2 with $\dot{m}_{air} / \dot{m}_{fuel} = 3$

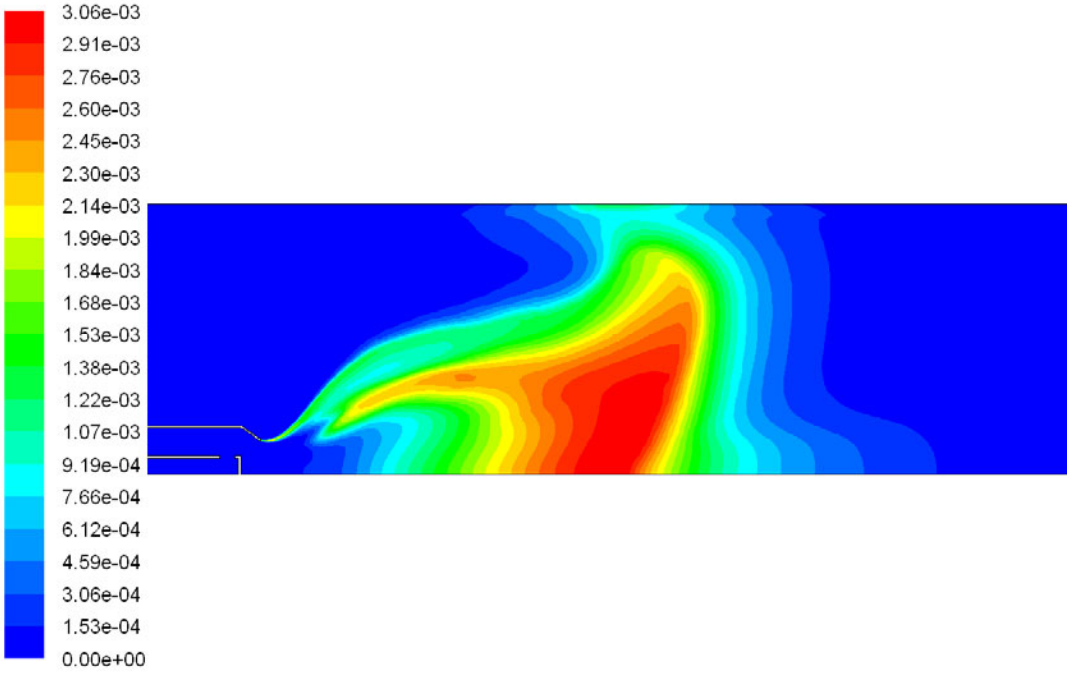

Figure 45: Contours of OH mole fraction, 10 kW @ 3% O_2 with $\dot{m}_{air}/\dot{m}_{fuel} = 3$

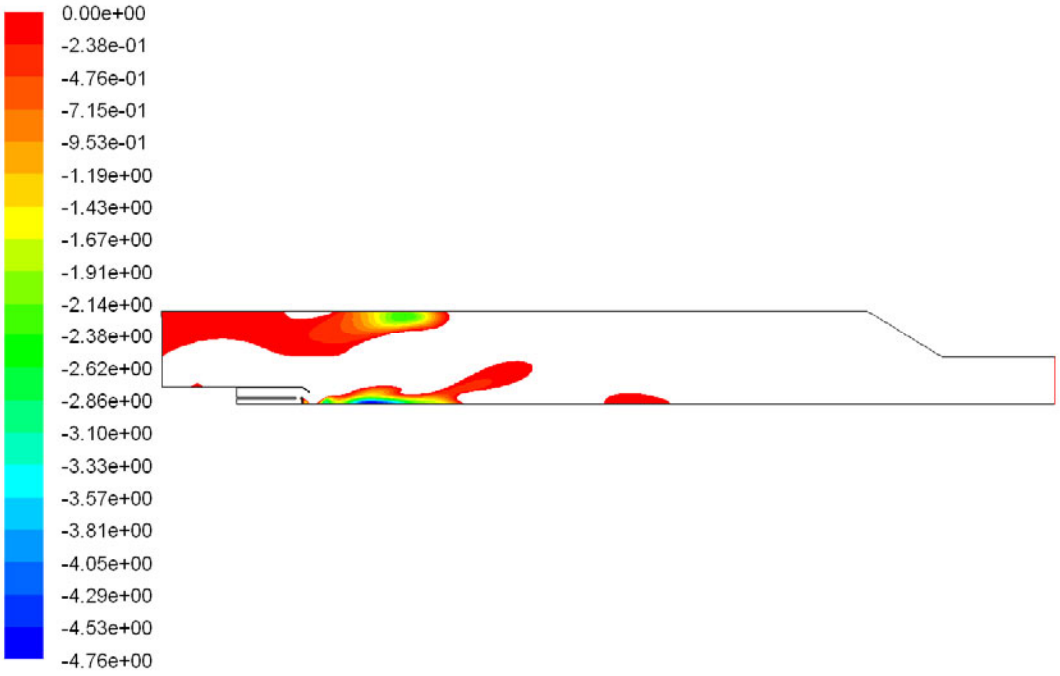

Figure 46: Contours of zero-axial velocities [m/s], 10 kW @ 3% O_2 with $\dot{m}_{air}/\dot{m}_{fuel} = 3$

B.7 Contours with premixed air-fuel ratio equal to 3.5

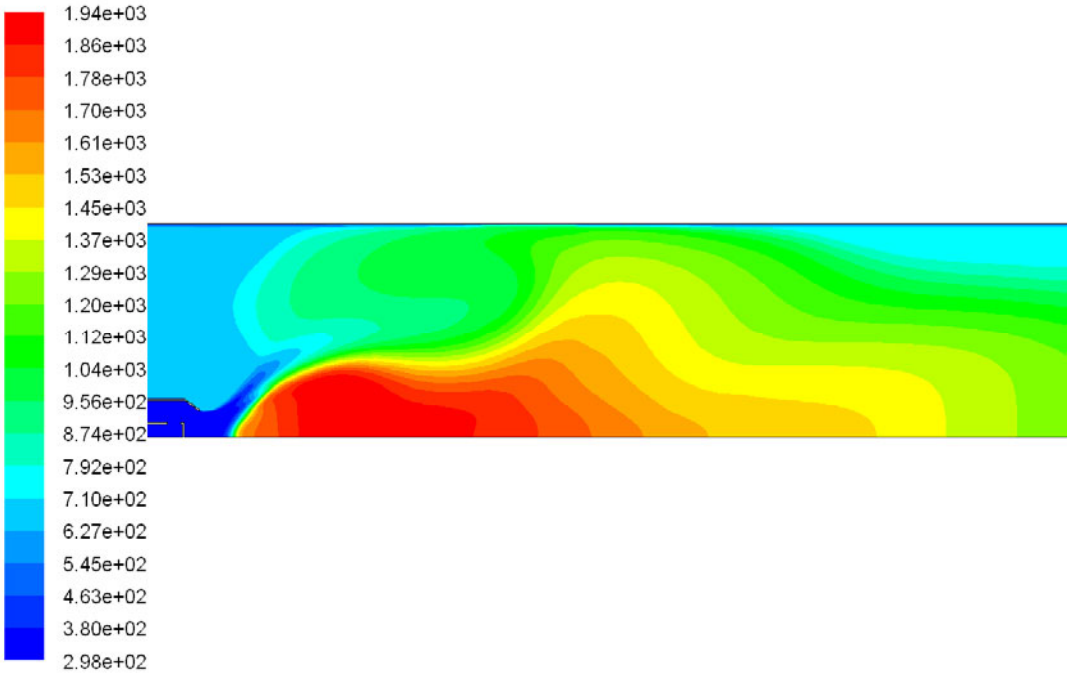

Figure 47: Contours of temperature [˚C], 10 kW @ 3% O_2 with $\dot{m}_{air} / \dot{m}_{fuel} = 3.5$

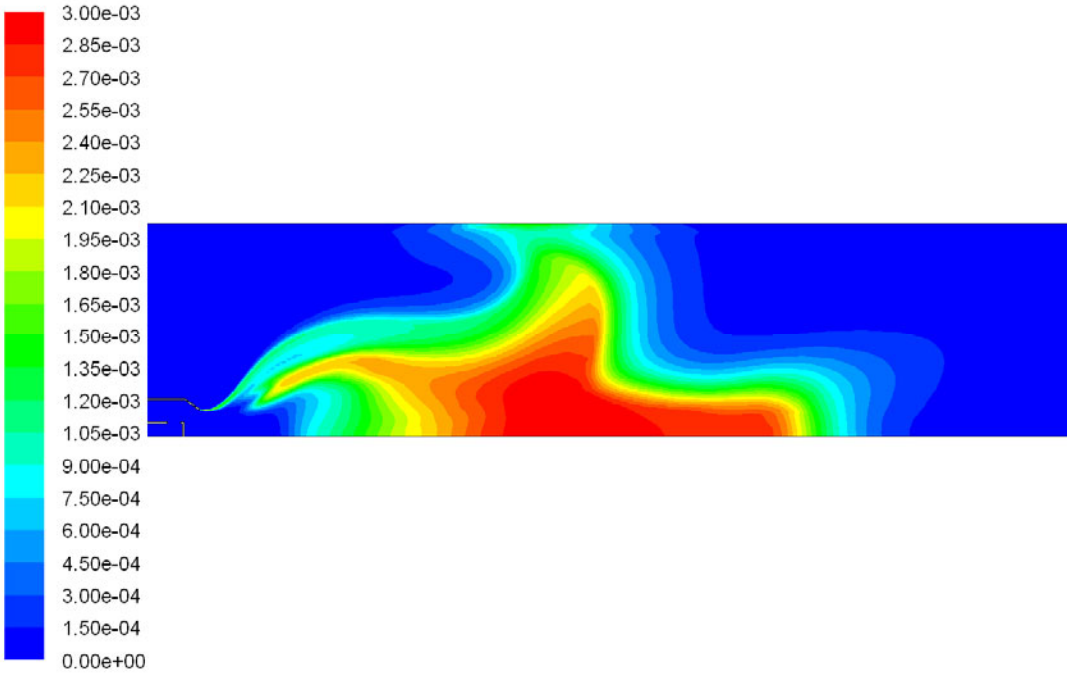

Figure 48: Contours of OH mole fraction, 10 kW @ 3% O_2 with $\dot{m}_{air} / \dot{m}_{fuel} = 3.5$

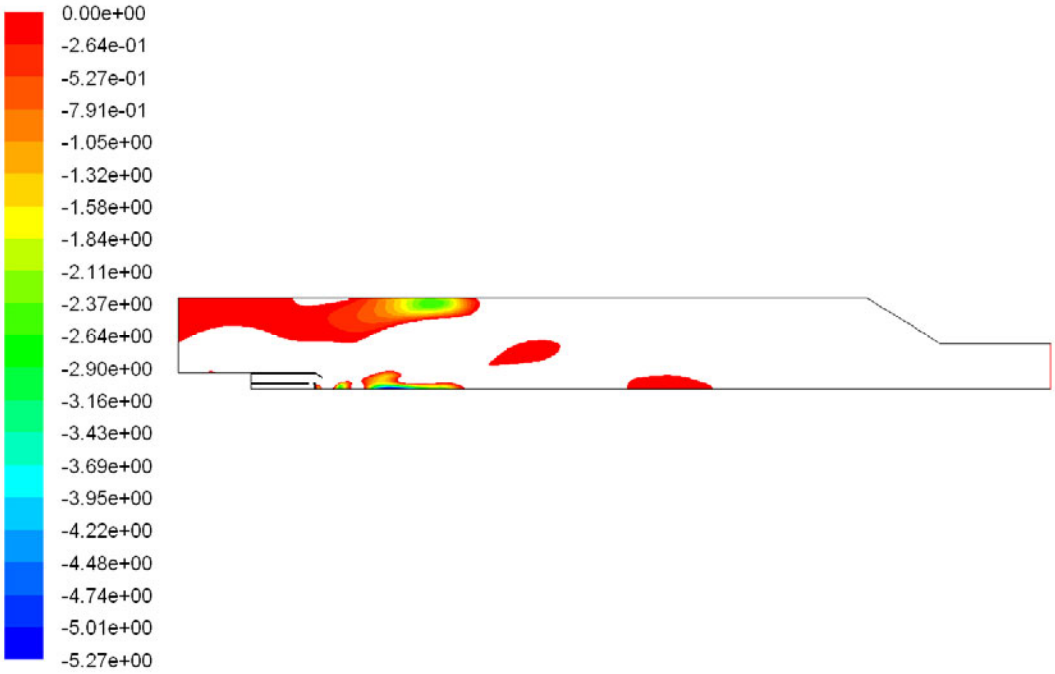

Figure 49: Contours of zero-axial velocities [m/s], 10 kW @ 3% O_2 with $\dot{m}_{air}/\dot{m}_{fuel} = 3.5$

B.8 Contours with premixed air-fuel ratio equal to 4

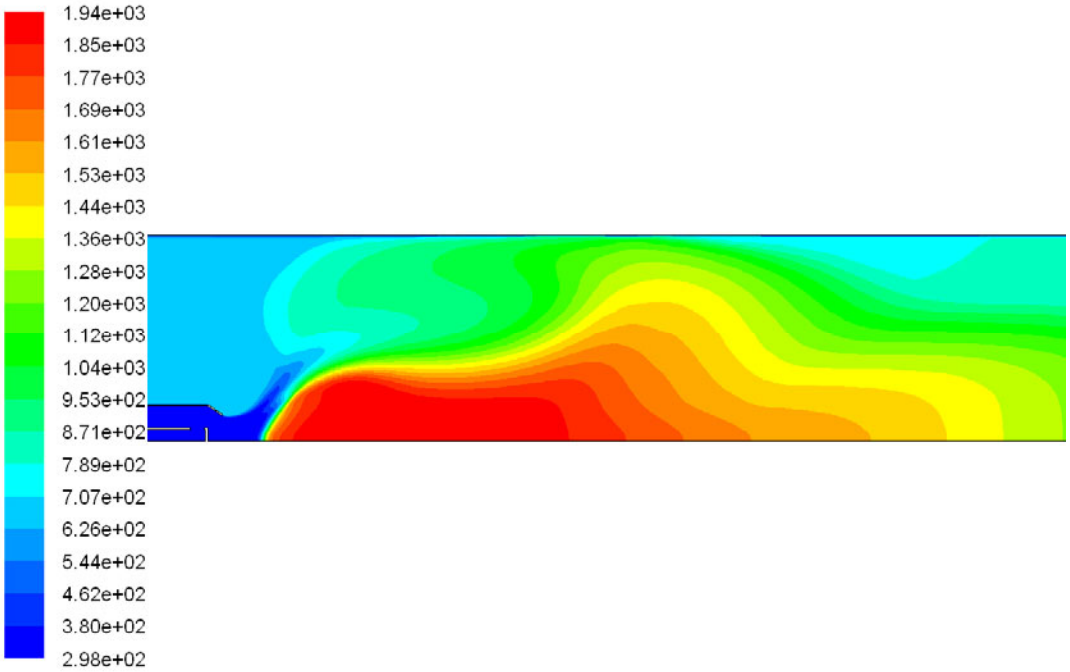

Figure 50: Contours of temperature [˚C], 10 kW @ 3% O_2 with $\dot{m}_{air}/\dot{m}_{fuel} = 4$

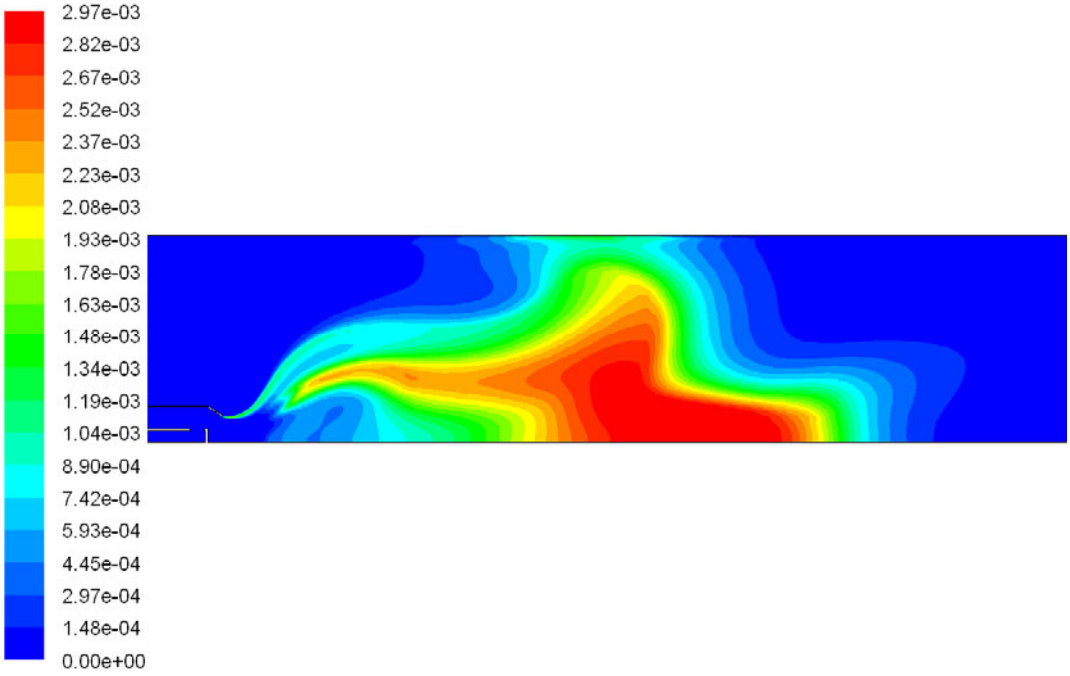

Figure 51: Contours of OH mole fraction, 10 kW @ 3% O_2 with $\dot{m}_{air}/\dot{m}_{fuel} = 4$

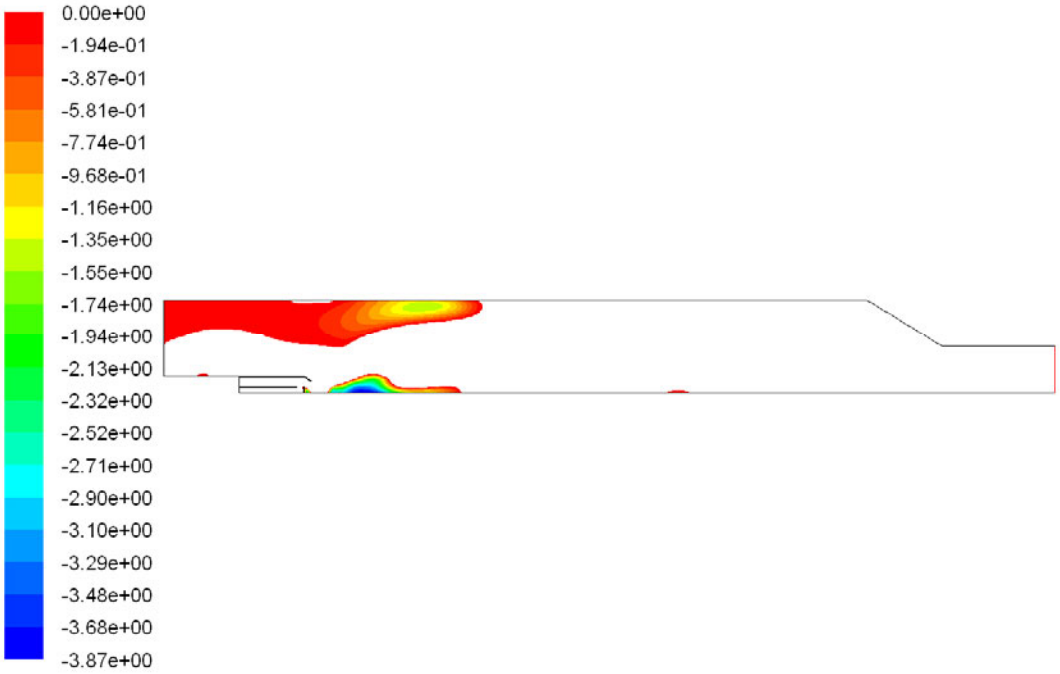

Figure 52: Contours of zero-axial velocities [m/s], 10 kW @ 3% O_2 with $\dot{m}_{air}/\dot{m}_{fuel} = 4$

B.9 Comparison of HCN concentration at different air-fuel ratios

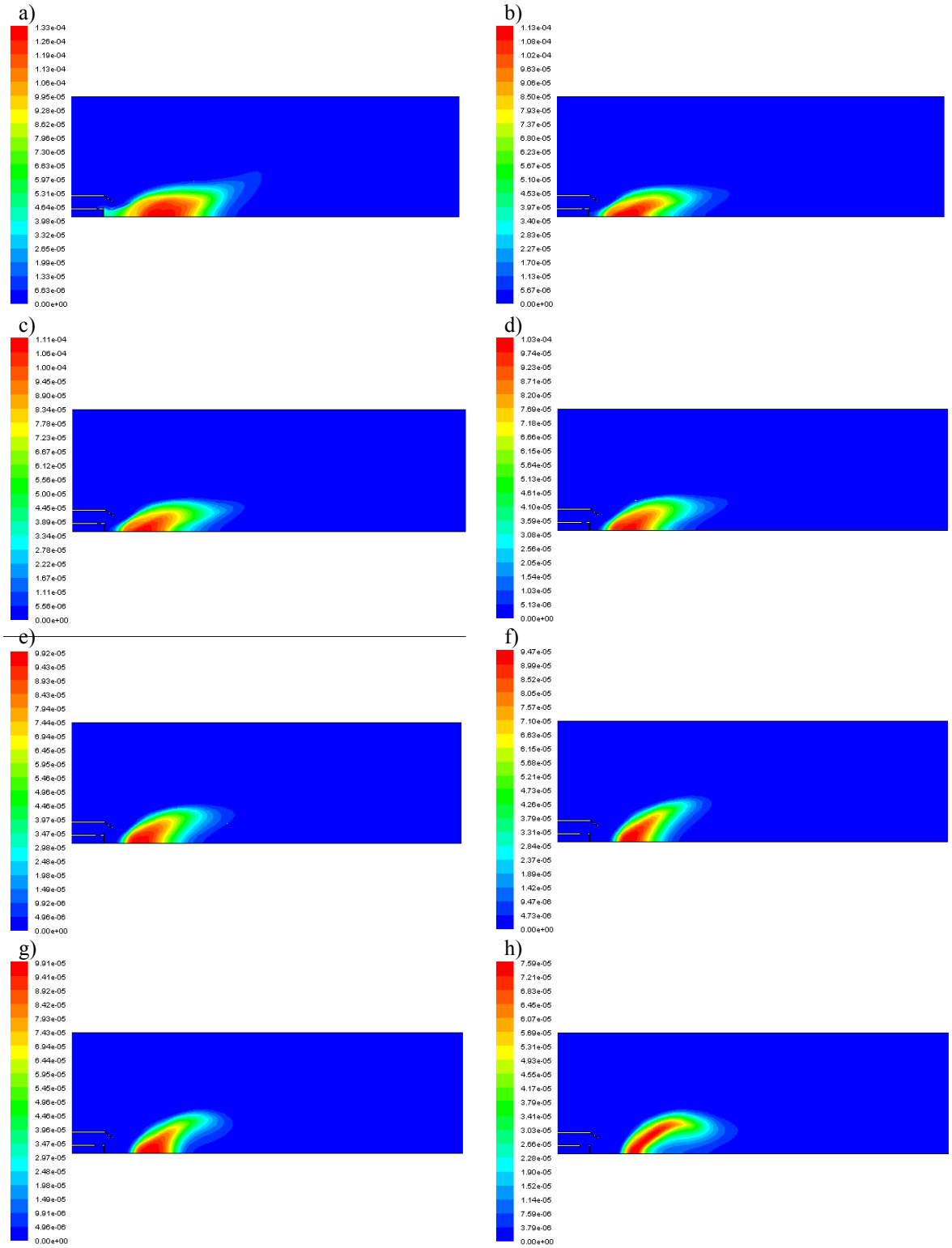

Figure 53: Contours of HCN mole fraction for air-fuel ratios of: a) 0; b) 0,5; c) 1; d) 1,5; e) 2; f) 3; g) 3,5; h) 4

Appendix C Pictures of the 20 kW swirl burner

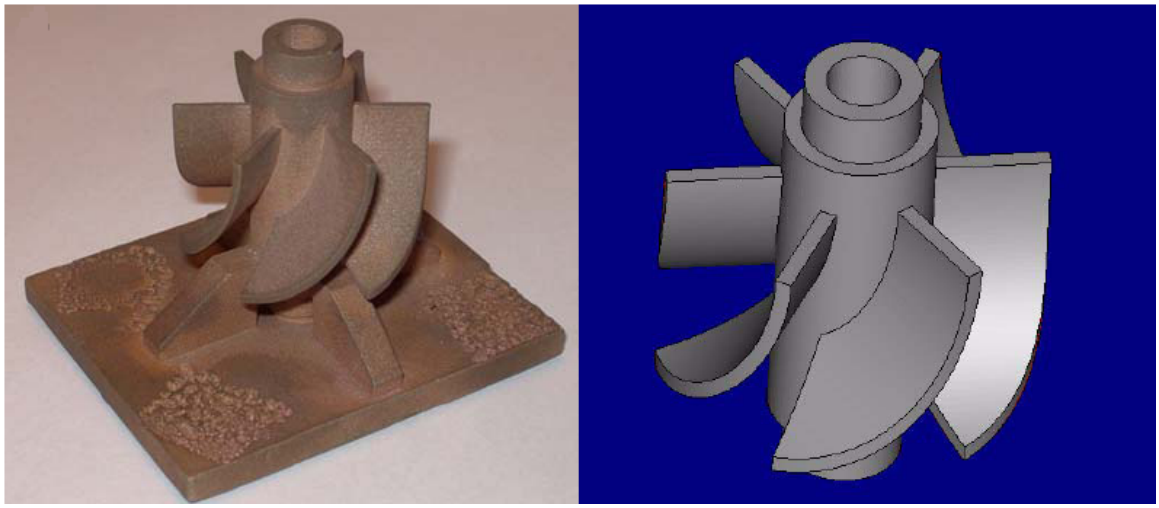

Figure 54: The swirl generator [3]

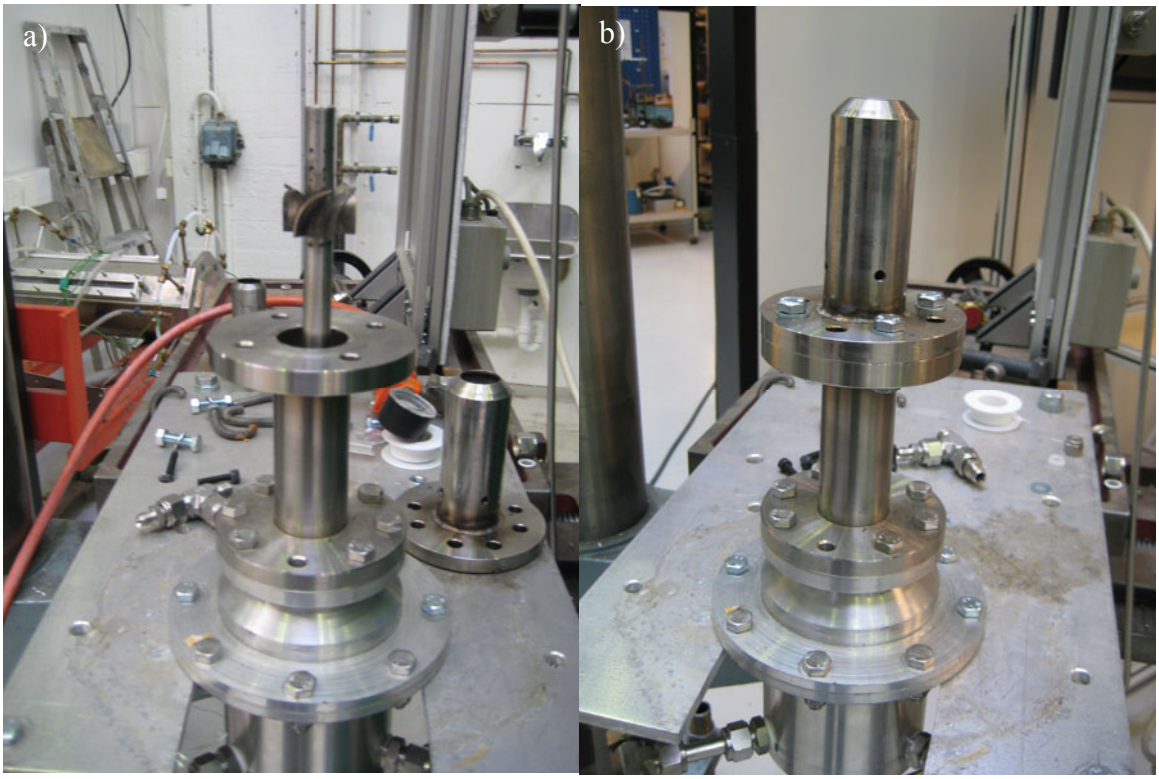

Figure 55: a) The gas tube without the burner tube and the combustion chamber b) The burner without the combustion chamber

Figure 56: The combustion chamber

Appendix D Enclosed DVD

The enclosed DVD contains the following:

- The GRIMECH 3.0 formation mechanism [26]
- Excel sheet with an overview of the geometry of the 20 kW swirl burner
- Excel sheet with the results from the simulations
- GAMBIT and FLUENT files for all of the different air-fuel ratios

References

1. U.S. Environmental Protection Agency. *Health and Environmental Impacts of NOx*. [cited 2008 25.04]; Available from: http://www.epa.gov/airprogm/oar/urbanair/nox/hlth.html.
2. Statistics Norway, *Utslipp av nitrogenoksider, NMVOC, svoveldioksid og ammoniakk. 1990-2006*. 2008.
3. Spangelo, Ø., *Experimental and Theoretical Studies of a Low NOx Swirl Burner*, in *Department of Energy and Process Engineering*. 2004, Norwegian University of Science and Technology: Trondheim.
4. Turns, S.R.S.R., *An introduction to combustion : concepts and applications.*
5. De Nevers, N.N., *Air pollution control engineering.*
6. Ansys, *Fluent 6.3 User's Guide*. 2007.
7. Bozzelli, J.W. and A.M. Dean, *O + NNH: A possible new route for NOx formation in flames.* International Journal of Chemical Kinetics, 1995. **27**(11): p. 1097-1109.
8. Konnov, A.A., *On the relative importance of different routes forming NO in hydrogen flames.* Combustion and Flame, 2003. **134**(4): p. 421-424.
9. Kutz, M., *Mechanical engineers' handbook - Energy and Power*. 3rd ed.
10. Turns, S.R., et al., *Oxides of nitrogen emissions from turbulent jet flames: Part II--Fuel dilution and partial premixing effects.* Combustion and Flame, 1993. **93**(3): p. 255-269.
11. Cheng, T.S., et al., *Effects of partial premixing on pollutant emissions in swirling methane jet flames.* Combustion and Flame, 2001. **125**(1-2): p. 865-878.
12. Gore, J.P. and N.J. Zhan, *NOx emission and major species concentrations in partially premixed laminar methane/air co-flow jet flames.* Combustion and Flame, 1996. **105**(3): p. 414-418.
13. Xue, H. and S.K. Aggarwal, *NOx emissions in n-heptane/air partially premixed flames.* Combustion and Flame, 2003. **132**(4): p. 723-741.
14. Lyle, K.H., et al., *A study of pollutant emission characteristics of partially premixed turbulent jet flames.* Combustion and Flame, 1999. **116**(4): p. 627-639.
15. Dittrich, S., *Combustion of diluted fuels*, in *Department of Energy and Process Engineering*. 2007, Norwegian University of Science and Technology: Trondheim.
16. Rortveit, G.J., et al., *Effects of diluents on NOx formation in hydrogen. counterflow flames.* Combustion and Flame, 2002. **130**(1-2): p. 48-61.
17. Rørtveit, G.J., *NOx Emissions From Combustion of Hydrogen Mixtures*, in *Department of Energy and Process Engineering*. 2002, NTNU: Trondheim.
18. Baukal, C., *Everything you need to know about NOx: Controlling and minimizing pollutant emissions is critical for meeting air quality regulations.* Metal Finishing, 2005. **103**(11): p. 18-24.
19. Boyece, M.P., *Gas Turbine Engineering Handbook* 3rd ed, ed.
20. Moran, M.J.M.J., *Fundamentals of engineering thermodynamics.*
21. Røkke, N.A., Experimental and theoretical studies of environmental aspects of natural gas combustion, in Department of Energy and Process Engineering 1994, NTNU: Trondheim.

22. Incropera, F.P. and D.P. DeWitt, Fundamentals of heat and mass transfer. 2002.
23. Ertesvåg, I.S., Turbulent strøyming og forbrenning: frå turbulensteori til ingeniørverkty. 2000, Trondheim: Tapir trykk. 294.
24. White, F.M., Fluid mechanics. 2003.
25. Frassoldati, A., et al., Determination of NOx emissions from strong swirling confined flames with an integrated CFD-based procedure. Chemical Engineering Science, 2005. **60**(11): p. 2851-2869.
26. Smith, G.P., et al. GRI-MECH 3.0. 2008 [cited 2008 04.03]; Available from: http://www.me.berkeley.edu/gri_mech/.